Technische Universität Wien

DIPLOMARBEIT

Aperture–Coupled Microstrip Patch Antenna Array

ausgeführt am Institut für

Nachrichtentechnik und Hochfrequenztechnik

der Technischen Universität Wien

von

Alexander Kuchar

Friedhofallee 4a/11

A-2232 Deutsch–Wagram

March 15, 1996

_____

Betreuer:
Mag. Dipl.-Ing. Josef Fuhl
o.Univ.Prof. Dipl.-Ing. Dr. Ernst Bonek

Abstract

Microstrip patch antennas get more and more important in these days. This is mostly due to their versatility in terms of possible geometries that makes them applicable for many different situations. The lightweight construction and the suitability for integration with microwave integrated circuits are two more of their numerous advantages. Additionally the simplicity of the structures makes this type of antennas suitable for low–cost manufacturing. And this is also one key–feature why microstrip patch antennas are used in mobile communications applications.

The aim of this work is to design and to implement a microstrip patch antenna array that meets the requirements of a base station antenna in a mobile communications system. The array needs no conventional beamforming network, because it will function as a digital controlled phased array. The array consists of nine linearly arranged single antennas with an element spacing of half a free–space wavelength.

The antenna was designed to operate in the ISM–band at 2.45GHz, where the required bandwidth is 83.5MHz. Since microstrip patch antennas have a low bandwidth, a special feeding technique — aperture–coupling — was implemented. This technique makes it possible to use a low–permittivity patch substrate with a large thickness. With this configuration a broadband microstrip patch antenna can be realized.

For the design of the antenna a simulation tool based on the Method of Moments was used. After optimizing and implementing a single element antenna that achieved satisfactory measurement results, the antenna array was worked out.

The excellent final results for the antenna array — a bandwidth of 160MHz, a front–to–back ratio larger than 17dB, and a maximum mutual coupling below -14.5dB — is another proof that aperture–coupled microstrip patch antennas are suitable for the operation in a mobile communications system.

Zusammenfassung

Mikrostreifenleitungsantennen gewinnen durch ihre flexible Geometrie und der damit verbundenen vielseitigen Anwendbarkeit immer mehr an Bedeutung. Die Leichtbauweise und die Möglichkeit des gemeinsamen Einsatzes mit integrierten Mikrowellenschaltungen sind zwei weitere Vorteile. Zusätzlich bedeutet die Einfachheit der verwendeten Struktur niedriegere Produktionskosten und motiviert daher die Verwendung von Streifenleitungsantennen in der Mobilkommunikation.

Das Ziel der vorliegenden Arbeit ist der Entwurf und die Implementierung einer Antennengruppe, die den Anforderungen einer Basisstationsantenne für ein modernes Mobilkommunikationssystem gerecht wird. Aufgrund der digitalen Steuerung der Antennengruppe wird kein Speisenetzwerk benötigt. Die Antennengruppe besteht aus neun linear angeordneten Streifenleitungsantennen, wobei der Elementabstand eine halbe Wellenlänge beträgt.

Die Antenne ist für das ISM–Band bei 2.45GHz entwickelt, wobei eine Bandbreite von 83.5MHz gefordert ist. Wegen der Schmalbandigkeit von Mikrostreifenleitungsstrukturen wird die Antenne mittels eines Schlitzes gespeist, wodurch ein dickes schaumartiges Substrate mit sehr niedriger Permittivität verwendet werden kann. Erst diese Speiseart macht eine breitbandige Mikrostreifenleitungsantenne möglich.

Die Konstruktion der Antenne wurde mit Hilfe eines auf der Momentenmethode basierenden Simulationsprogramms durchgeführt. Nachdem mit einem optimierten Einzelantennenelement die geforderten Eigenschaften erreicht wurden, konnte die Antennengruppe entwickelt werden.

Die hervorragenden Meßergebnisse für die endgültige Antennengruppe — eine Bandbreite von $160MHz$, ein Vor–Rückverhältnis von mehr als $17dB$ und eine maximale Strahlungskopplung von -14.5dB — beweisen, daß schlitzgekoppelte Streifenleitungsantennen für den Einsatz in einem Mobilkommunikationssystem geeignet sind.

Preface

Today's mobile communications research and development are heading against a third generation mobile communications system, called UMTS — **U**niversal **M**obile **T**elecommunications **S**ystem and IMT–2000 — **I**nternational **M**obile **T**elecommunications system. One key feature of such a mobile communications system should be its superior capacity. To fulfill these future capacity requirements new access schemes have to be implemented. Second generation mobile communications systems, like GSM (**G**lobal **S**ystem for **M**obile **C**ommunications), often use a combination of FDMA (**F**requency **D**ivision **M**ultiple **A**ccess) and TDMA (**T**ime **D**ivision **M**ultiple **A**ccess) as access–technique. A new approach is to allow another additional access domain — the space. This technique is called SDMA — **S***pace* **D***ivision* **M***ultiple* **A***ccess* — and tries to take advantage of the different locations of the users.

Such a system utilizes the concept of ADAPTIVE ANTENNAS at the base station. The antenna pattern is continuously adapted to the actual situation of the mobile user distribution to enhance capacity. This continuous adapting of the antenna pattern requires an algorithmic controlled phased array. Or, in other words — the system works with an antenna array whose pattern characteristic can be electronically varied.

The workgroup of mobile communications at the INTHF[1] is currently implementing such an adaptive antenna system — named AdAnt. As a part of this team, the aim of my work was the implementation of an antenna array in microstrip technology that is suitable for the operation in such an environment.

Chapter 1 of this thesis includes an introduction and the requirements for the antenna, while Chapter 2 gives a brief discussion of the theoretical background of microstrip patch antennas. Here the emphasis lies on the most important subjects to provide you with enough basic knowledge and citations to follow the essentials of this work.

Today an antenna engineer can fortunately choose from a variety of simulation tools for solving electromagnetic problems that prevent the necessity of applying time–consuming try–and–error methods. For this work I used a low–price simulation package that nevertheless gave excellent results. In Chapter 3 I will report about the functionality of the simulation tool and about the implemented simulation machine. In this

[1] Institut für Nachrichtentechnik und Hochfrequenztechnik, Technische Universität Wien
Gußhausstraße 25/389, A–1040 Wien, Austria

chapter I will also report on the experience I made by using this tool.

The last two chapters summarize the actual work. To gain control of the design of microstrip antennas the first step was the implementation of a single antenna array; and only until I achieved satisfying results with the single element antenna, I focused on the implementation of an antenna array. Chapter 4 is dedicated to the discussion of the single antenna, while Chapter 5 includes the antenna array. Both chapters explain the design steps and the implementation of the physical antenna. They also include the measurement results, the comparison of these results with the theoretical expectations and further conclusions.

Acknowledgment

I want to express my thanks to Hans–Oliver Ruoss and his colleagues from the Institut für Hochfrequenztechnik in Stuttgart, with whom I spent a whole day in measuring the antenna array in their anechoic chamber.

I owe special thanks to Richard C. Hall from Boulder Microwave Technologies for simulating the final antenna array with BMT's simulation tool **Ensemble**. I am grateful for his patience in fulfilling all my wishes for always further and further simulation results.

I want to thank Prof. Dr. Splitt for the fruitful discussions about his simulation tool **MultiStrip**.

I also want to thank Mr. Josef Rubin from Thun–Hohenstein GmbH, who supplied us with free sample sheets of the foam material Rohacell.

Support of this work by the Austrian PTT is gratefully acknowledged.

Contents

List of Figures

List of Tables

Chapter 1

Introduction

For a mobile communications system the technique of printed antennas seems to have numerous advantages (see Section 2.2.1). Therefore printed antennas get more and more important in the field of antenna design. This lead us to the decision to implement a microstrip patch antenna.

The following section gives a brief discussion of the AdAnt system with emphasis on the RF–part to end up with a list of requirements for the antenna array.

1.1 Block Diagram

Figure 1.1 shows the simplified block diagram of the AdAnt system. On the left–hand side you find the antenna array with its nine elements, each connected to the input of one of the nine transceiver front ends. Each antenna element output signal is downconverted to baseband and sampled to digital signals (in the receive mode and vice versa in the transmit mode). These signals are further passed to a digital signal processor unit. Here they are weighted and combined, this means that the antenna pattern[1] is formed by means of software. This *'software pattern'* is controlled by an adaptive algorithm. Figure 1.2 shows a simplified scenario with two mobile users in cell A. Two different antenna patterns (solid and dashed line) serve one mobile user each at the same time slot *and* the same frequency. That is what we basically call SDMA. The superior performance compared to systems without SDMA comes from the following fact: The signal intended for user B (dashed line) causes interference for user A. This interference is minimized by forcing the antenna pattern dedicated to user B to have a null in the direction of user A and vice versa. Again, this is just one possible philosophy to improve the communication situation for the mobiles. But this example gives you an idea how to exploit the different locations of the individual users.

Up to know, I have always written 'adaptive' algorithm, but never named any

[1] There are various philosophies in consideration to derive an optimum antenna pattern, and even some algorithms do not take care of the pattern explicitly. Instead, they may maximize the signal–to–noise ratio or any other important performance parameter.

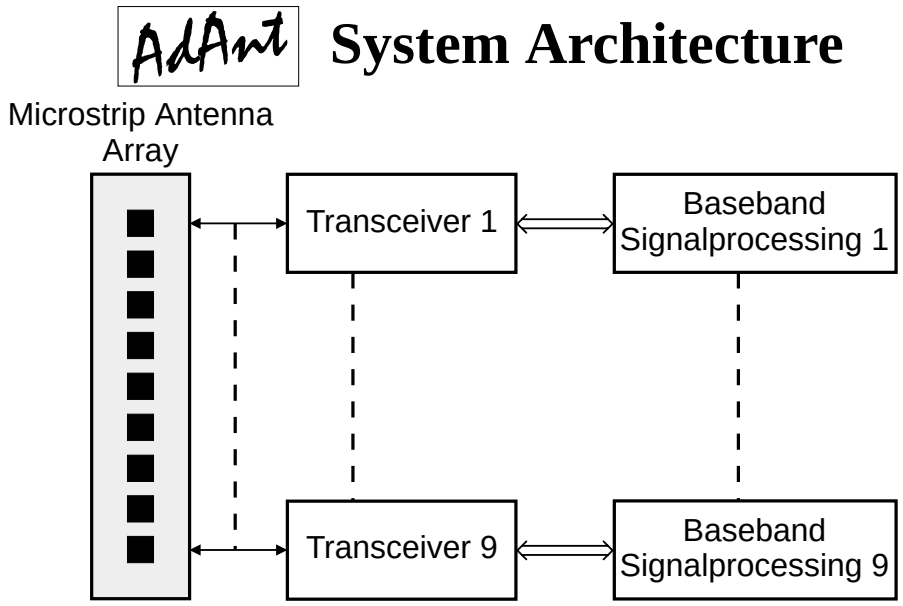

Figure 1.1: Block diagram of the AdAnt system.

explicitly. This is because the major motivations for this project are: (a) to prove that adaptive antennas work, and (b) to determine the performance of several algorithms that are capable for such problems (like LMS (**L**east **M**ean **S**quares), RLS (**R**ecursive **L**east **S**quares), SQRLS (**S**quare **R**oot RLS), DMI (**D**irect **M**atrix **I**nversion), Wiener filter and CMA (**C**onstant **M**odulus **A**lgorithm) — for details see [8]).

A consequence of this signal combination concept is that the antenna array does not require any hardware beamforming network.

1.2 Requirements for the Antenna Array

From this concept the following requirements for the antenna are derived:

1.2.1 Array Element Number

One of the first questions that arose was: *How many antenna elements shall be implemented?*

Of course, the higher the number of elements, the better is the performance[2] of such a system. Unfortunately, hand in hand with increasing the element number the *cost* and the *computational load* increase too. We decided to realize a nine element

[2]With performance I mean for example the angular resolution of the antenna array.

array, because based on this number even a three–by–three planar array can be build up. Although, I want to state that this work addresses the implementation of a nine element *linear* array only.

1.2.2 Operating Frequency Band — Operating Bandwidth

A main property of a mobile communications system is its operating frequency band. Here we decided to use the ISM (**I**ndustrial **S**cientific **M**edical)–band at 2.45GHz. The exact location of the frequency band is [7]

$$\text{ISM–band:} \qquad 2400MHz \ldots 2483.5MHz. \tag{1.1}$$

This leads to a bandwidth of

$$BW = 83.5MHz \qquad \text{or} \qquad RBW = 3.4\%,$$

where BW is the absolute bandwidth and RBW is the relative bandwidth, defined as

$$RBW = \frac{BW}{f_c}$$

with $f_c = 2.45GHz$ as the center frequency of the ISM–band.

Since the antenna shall operate within the whole ISM–band the required bandwidth of the antenna array is given by the ISM–bandwidth. In this work the bandwidth is defined as the frequency range where the antenna inputs are matched to 50Ω. By definition an microwave component is matched when the Voltage–Standing–Wave Ratio $VSWR \leq 2$. A relative bandwidth of 3.4% is for a microstrip patch antenna a broadband case and therefore a special technique to fulfill this requirement has to be used (see Section 2.3).

1.2.3 Array Element Spacing

Another requirement for the array is that the distance[3] between two neighbouring elements is smaller than or equal to half of the smallest free–space wavelength λ_{0min} within the ISM–band

$$\lambda_{0min} = \frac{c_0}{f_{upper}} = 120.7mm,$$

and therefore

$$d_{max} \leq 60.35mm,$$

[3]This distance — subsequently called spacing — is measured from the center of one feeding point to the next.

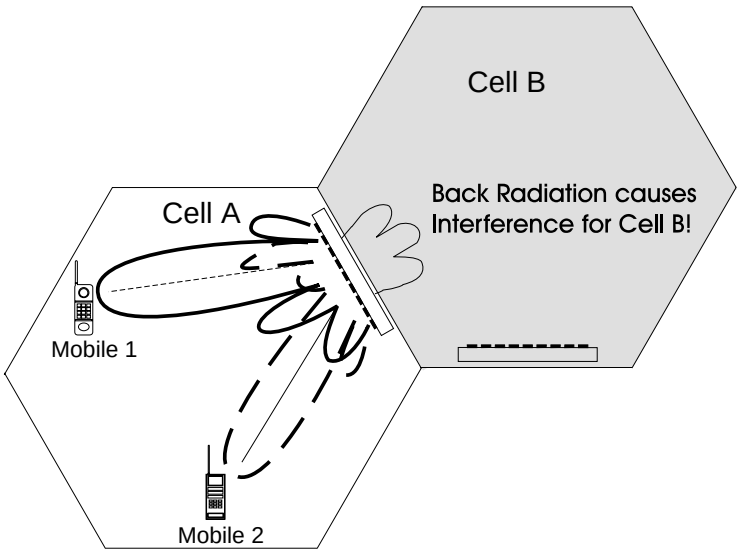

Figure 1.2: Base station antenna operating in a cellular environment.

where d_{max} is the maximum permitted element spacing and f_{upper} is the upper frequency band limit of the ISM–band. This requirement comes from the fact that from uniform array theory the maximum spacing allowed to avoid ambiguity is given by [15]

$$\frac{d_{max}}{\lambda_0} \leq \frac{1}{1+\sin\Theta_0}, \tag{1.2}$$

where Θ_0 is the scan angle measured from the antenna broadside and λ_0 is the free–space wavelength. To scan the whole hemisphere ($|\Theta_0| \leq 90°$) without ambiguity the maximum spacing is

$$d_{max} = 0.5\lambda_0. \tag{1.3}$$

Compared to conventional arrays, which use a spacing in the range of $(0.7 \ldots 0.8)\lambda_0$[4], with a spacing of $0.5\lambda_0$ considerable attention has to be directed to the minimization of the mutual coupling (see Chapter 5).

1.2.4 Back Radiation

Since a mobile communications system uses a cellular structure, an important requirement is the minimization of interference to neighbouring cells. So we need a base station antenna that minimizes the radiation into neighbouring cells, this means to maximize the front–to–back ratio (see Figure 1.2).

[4]This range is optimum in terms of directivity and angular resolution.

To maximize the front–to–back ratio, I introduced a reflector behind the antenna structure (see Section 2.3.2).

In this context I want to define the front–to–back ratio F/B as I will use it in this work:

$$F/B = 10 \log_{10} \frac{\iint_{\Omega_{upper}} \mid F(\phi,\theta) \mid^2 d\Omega}{\iint_{\Omega_{lower}} \mid F(\phi,\theta) \mid^2 d\Omega} \tag{1.4}$$

where $F(\phi,\theta)$ is the normalized field pattern of the antenna, θ and ϕ are the elevation and azimuth and Ω_{upper} and Ω_{lower} are the solid angles for the upper and the lower hemisphere, respectively. In this definition the numerator equals the power that is radiated into the upper hemisphere, while the denominator equals the power that is radiated into the lower hemisphere. Here it is assumed that the ground plane of the antenna lies in the horizontal plane ($\Theta = 90°$). Note that although this definition for the front–to–back ratio is in terms of solid angle — and so for a three–dimensional pattern — I will use it only for a two–dimensional antenna pattern (in my case $\phi = const.$). In this case, both double–integrals are downsized to single integrals over the corresponding angular regions and don't correspond to radiated powers anymore.

Many antenna engineers compute the front–to–back ratio by dividing the directivity (or the maximum power gain) by the directive gain (or the power gain) in a specified direction towards the back. With the type of antenna I have realized there is no certain meaningful direction towards the back. Usually one would use the direction of the maximum power gain. But as you will see in the results, the maximum power gain at the back of the antenna occurs near the ground plane and not broadside. With this information I decided to use the above mentioned definition for the front–to–back ratio, since it is clear and comprehensible.

1.2.5 Polarization

Finally we want to use a linear polarized antenna. As an option for future systems a microstrip antenna with dual polarization can also be implemented, where polarization diversity can be utilized. Therefore I also have to observe the polarization purity of the designed antenna.

1.2.6 Summary of Requirements

The following list summarizes the requirements for the antenna:

- linear antenna array with nine elements
- linear polarized
- element spacing: $\leq 60.35mm$
- operation frequency band: $2400MHz \ldots 2483.5MHz$

- bandwidth: $> 83.5MHz$
- 50Ω–system
- front–to–back ratio: $> 15dB$
- polarization purity: possibly high
- mutual coupling: possibly $< -10dB$

Chapter 2

Theory

This chapter should give you basic knowledge of microstrip patch antennas, of course with the emphasis in this work on broadband aperture–coupled microstrip patch antennas.

Although the following list of publications does not call on completeness, it should help you to get the fundamentals in order to understand this work.

2.1 Literature

The concept of printed antennas was originally proposed by Deschamps in 1953 [6]. However, it took more than twenty years until Munson realized the first microstrip antenna [18]. In 1979 an antenna symposium held in New Mexico initiated an international interest in microstrip antennas. A collection of papers presented at this meeting appeared in a special issue of the IEEE Transactions on Antennas and Propagation [5].

One of the first books that summarizes the topic of microstrip antennas, and which is still a standard reference, was written by Bahl and Bhartia [1]. Two excellent collections of articles can be found in [9] and recently in [23]. While [9] covers more the analysis aspect, [23] emphasizes on the design of microstrip antennas.

These above mentioned sources provide you a broad knowledge in printed antennas, while the following publications focus more on microstrip patch antenna techniques used in this thesis.

The pioneering work in the field of *aperture–coupled* microstrip patch antennas was published by Pozar [21]. Later publications about the theory of this feeding technique are given in [13], [22], [30], and [31]. Applications of aperture–coupled microstrip patch antennas are presented in [24] and [25].

An easy to read introduction to the state–of–the–art of *broadband* patch antennas is given in the book from Zürcher and his colleagues [33], while the corresponding article can be found in [32].

On the basis of these references you should be able to increase your knowledge in the field of microstrip patch antennas at least up to a level to understand this work.

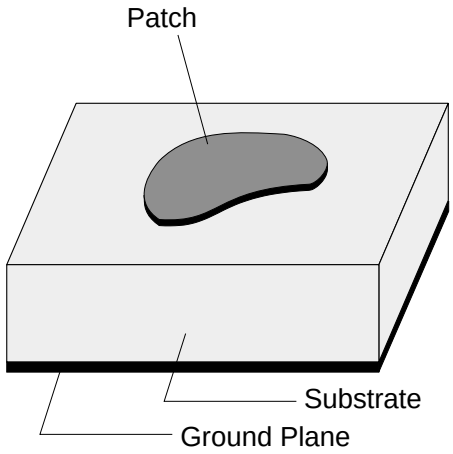

Figure 2.1: Microstrip antenna configuration.

2.2 Microstrip Antennas

A microstrip antenna is defined as [4]:

> *An antenna which consists of a thin metallic conductor bonded to a thin grounded dielectric substrate.*

Figure 2.1 shows a microstrip antenna in its simplest configuration. The antenna consists of a radiating patch on one side of a dielectric slab and a ground plane on the other side.

The patch, usually of copper, can have any shape, but rectangular and circular (elliptic) patches cover all possibilities in terms of pattern, bandwidth and polarization [16]. Even in terms of gain they exhibit a great versatility due to a possible range from 4 to 10dBi. These basic patch configurations also show up with their simple analysis and performance prediction. Because the rectangular patch fits the already mentioned requirements and is the easiest to handle, I will focus on this configuration.

2.2.1 Advantages and Drawbacks

Although there is a tremendous number of advantages, I will only pick out the — for my opinion — most important ones:

- lightweight, low volume, low profile

  Printed circuits are thin and thus require less volume than their waveguide or coaxial counterparts. Due to the fact that printed antennas consist mainly of nonmetallic materials and due to the frequent use of foam materials as substrates, such antennas have an extremely low weight compared to conventional antennas.

- polarization

  With the versatility of patch geometries any polarization can be obtained. You can even realize antennas with multipolarization capability with single or multiple ports. These features can be exploited for dual polarization operation or polarization diversity.

- dual frequency antennas possible

- excitation technique

  Patches allow a lot of different excitation techniques to be used, compatible with any technology of the active circuitry and beamforming networks.

- suitable for integration with MICs (**M**icrowave **I**ntegrated **C**ircuits)

  This is important, since MICs are much easier to handle and less expensive than the alternative waveguides.

Beside these numerous technological merits, there is also an important economic reason that makes microstrip antennas attractive: Printed antenna technology is suitable for low–cost manufacturing, because photo etching and press machining are the lowest cost technologies for large scale fabrications.

Of course there are a few drawbacks: First of all there is a limitation in frequency. At low frequencies ($\approx 100MHz$), the need of a given thickness (in terms of λ) to achieve a high efficiency and bandwidth leads to bulky (but not necessarily heavy) radiators; at high frequencies, once more the (very small) thickness and the manufacturing accuracy[1] limit the capability for low–cost production.

Microstrip antennas are narrowband antennas compared to conventional microwave antennas, since the radiation is a consequence of a resonance. Nevertheless this drawback can be overcome by using thicker substrates with low permittivity (see Section 2.3).

One has to care about the power–handling capability of printed circuits in the high power stages of radar or in industrial equipment for microwave heating. But when signal amplitudes remain generally low, as for example as in mobile communications, they are an excellent candidate for employment.

Another fact is that the design engineer has always to keep an eye on losses (mainly dielectric and due to surface wave excitation), since this leads to a lower gain and a lower efficiency. By selecting low loss–tangent substrates the dielectric losses will not be a serious issue anymore.

Finally, for many practical designs, the advantages of microstrip antennas far outweigh their disadvantages and so lead to many system applications (for example see [17]), such as:

[1] Today for low–cost technology the limit is in the range of 30GHz–50GHz.

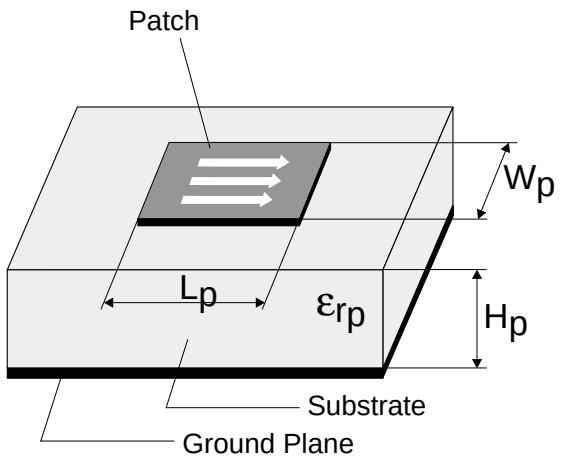

Figure 2.2: Rectangular patch antenna.

- mobile communications
- satellite communications
- remote sensing
- doppler radar, automotive radar, etc.

2.2.2 Microstrip Radiators

The heart of a microstrip antenna is the upper conductor — the patch (see Figure 2.2) — of finite dimensions. This patch can be considered to be an open–ended transmission line of length L_p and width W_p. The amplitude of the surface currents becomes significant when the signal frequency is close to resonance. By taking only the fundamental mode into account, the resonant frequency f_0 can be calculated by

$$f_0 = \frac{c_0}{2(L_p + 2\Delta L_p)\sqrt{\varepsilon_{eff}}}, \tag{2.1}$$

where ΔL_p is the equivalent length extension that accounts for the fringing fields at the two open ends, and ε_{eff} is the effective relative permittivity (see Equation 2.3). The last two parameters will be discussed in Section 2.2.3.

The question *how the patch radiates* arises now. To answer this, I will take a look at the electric field configuration. Thereby I assume that the patch is spaced a small fraction of a wavelength above the ground plane and that the electric field shows no variations along the width of the microstrip structure. Radiation may then be ascribed mostly to the *fringing fields* of the open–circuited edges of the patch (see Figure 2.3).

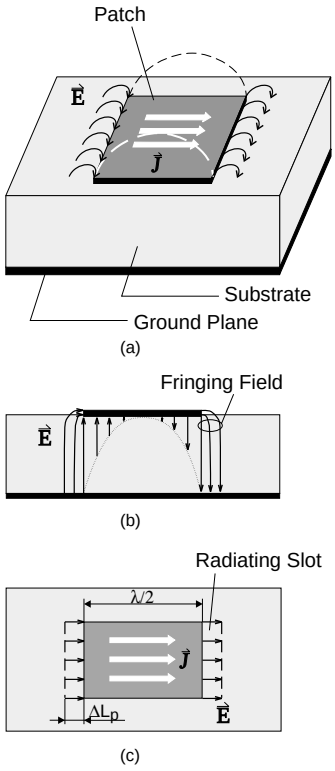

Figure 2.3: Field configuration of a microstrip patch antenna. (b) Side view. (c) Top view.

Finally I try to derive a simple radiation model: The fields at the end of the patch can be splitted into tangential and normal components with respect to the ground plane. The normal field components are out of phase because the length of the patch is approximately $\lambda/2$. Therefore their contribution to the far field in broadside direction cancel each other. The tangential field components, which are in–phase, combine to give the maximum radiated field normal to the surface of the patch. Therefore this structure can be modeled by two parallel slots, placed half a wavelength apart at the edges of the patch (see Figure 2.3 (c)). Obviously such an antenna is a broadside array. With this simple model the far–field pattern $F(\theta)$ in the H–plane can be analytically approximated by [1]

$$F(\theta) = \frac{\sin\left(\frac{\pi W_p}{\lambda_0}\sin\theta\right)}{\frac{\pi W_p}{\lambda_0}\sin\theta}\cos\theta. \tag{2.2}$$

This pattern approximation makes only sense for the upper hemisphere ($\mid \theta \mid \leq 90°$). Figure 2.4 shows $F(\theta)$ for a patch width $W_p = 0.4\lambda_0$.

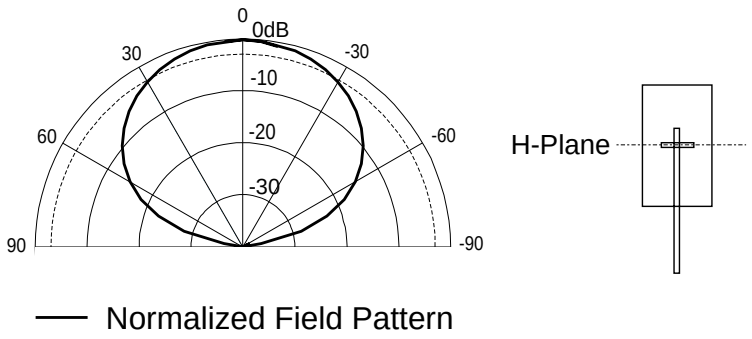

Figure 2.4: Simulation of the far–field by using a two slot model.

2.2.3 Microstrip Lines

As already mentioned, the microstrip antenna consists of an approximately half–wavelength microstrip line. Therefore the transmission line theory will be used to calculate the behaviour of such a structure, or in detail, to calculate important design parameters. Here I will present only the required results, since details about the transmission line theory can be found in almost any microwave book, for example see [2].

Effective Permittivity

A microstrip structure is not homogeneous because the electromagnetic field extends over two media: air and dielectric. Therefore wave propagation cannot be Transverse ElectroMagnetic (TEM), since waves in two medias travel with different velocities and the boundary conditions force non–zero transverse electric or transverse magnetic components. Nevertheless, the quasi–TEM approximation will be used, since longitudinal field components remain much smaller than the transverse ones.

The inhomogeneous microstrip line is replaced by an equivalent homogeneous line. The conductor retains the same geometry (W is the width of the microstrip line and H is the height of the dielectric) but is surrounded by a homogeneous dielectric of effective permittivity ε_{eff}, whose value is determined by evaluating the capacitance of the fringing field [10]

$$\varepsilon_{eff} = \frac{\varepsilon_r + 1}{2} + \frac{\varepsilon_r - 1}{2}\left(1 + 10\frac{H}{W}\right)^{-ab}, \tag{2.3}$$

with

$$a = 1 + \frac{1}{49}\ln\frac{\left(\frac{W}{H}\right)^4 + \left(\frac{1}{52}\frac{W}{H}\right)^2}{\left(\frac{W}{H}\right)^4 + 0.432} + \frac{1}{18.7}\ln\left[1 + \left(\frac{1}{18.1}\frac{W}{H}\right)^3\right] \qquad b = 0.564\left(\frac{\varepsilon_r - 0.9}{\varepsilon_r + 3}\right)^{0.053},$$

where ε_r is the relative permittivity of the substrate and $\ln(\cdot)$ denotes the natural logarithm. In this context I also want to define the later used effective, also called guide, wavelength

$$\lambda_{eff} = \frac{\lambda_0}{\sqrt{\varepsilon_{eff}}}. \tag{2.4}$$

Characteristic Impedance

The characteristic impedance Z_c for an infinitely thin strip can be approximated[2] by

$$Z_c = \frac{1}{2\pi}\sqrt{\frac{\mu_0}{\varepsilon_0\varepsilon_{eff}}}\ln\left(F_1\frac{H}{W} + \sqrt{1+\left(\frac{2H}{W}\right)^2}\right) \tag{2.5}$$

with

$$F_1 = 6 + (2\pi - 6)\exp\left[-\left(30.666\frac{H}{W}\right)^{0.7528}\right],$$

where ε_0 and μ_0 are the free–space permittivity and permeability, respectively.

Equations (2.3) and (2.5) connect the physical parameters (W, H and ε_r) with the electrical parameters (ε_{eff} and Z_c). But in the design procedure, I want to obtain a specific characteristic impedance (with a given substrate height and relative permittivity), and therefore I have to search for the proper strip width. So, I have to use an iterative procedure to solve this problem.

Open–Ended Transmission Line

A last parameter for calculating the resonant frequency of the patch (see Equation 2.1) has to be derived — the equivalent length extension of the patch ΔL_p.

The electric field of an open microstrip line does not end abruptly (see Figure 2.3) at the edge of the patch, but extends slightly beyond. To account for this so called fringing field, one can either introduce a capacitance or an equivalent length extension [33]

$$\Delta L_p = 0.412 H_p \frac{\varepsilon_{eff} + 0.3}{\varepsilon_{eff} - 0.258}\frac{W_p/H_p + 0.262}{W_p/H_p + 0.813}. \tag{2.6}$$

2.2.4 Surface Waves

The purpose of an antenna is of course to radiate space waves. These are waves that move towards the free space where they do not find any further interfaces. Thus, the power of a space wave decreases with distance r as $1/r^2$.

[2] The accuracy for this approximation is reported as 0.03% over the range $0 \leq W/H \leq 1000$ [33].

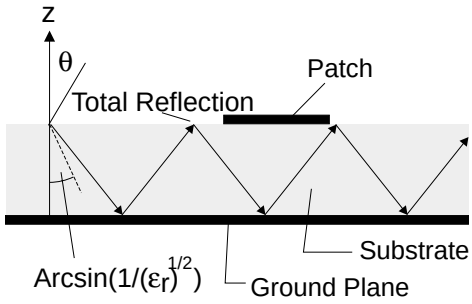

Figure 2.5: Surface waves.

But, there are also other types of waves excited in an antenna that are unwanted. The most important one are the surface waves. These waves propagate slightly downwards from the patch into the patch substrate, having an elevation angle θ between

$$\pi/2 \leq \theta \leq \pi - \arcsin\left(1/\sqrt{\varepsilon_{r_p}}\right). \tag{2.7}$$

Then the wave hits the ground plane, where it is reflected, it hits the dielctric–to–air boundary and is again reflected, and so on (see Figure 2.5). Some discrete surface wave modes are excited, whose power decreases only with $1/r$ with increasing distance. Both Transversal Magnetic (TM) and Transversal Electric (TE) surface waves can be excited on a grounded dielectric substrate. The cutoff frequency f_c of these modes is given by [20]

$$f_c = \frac{nc}{4H\sqrt{\varepsilon_{r_p} - 1}}, \tag{2.8}$$

where c is the speed of light, and $n = 0, 1, 2, 3, \ldots$ for the TM_0, TE_1, TM_2, ...surface modes. Note that the TM_0 mode has zero cutoff frequency, so that it can be generated for any substrate thickness H. As the substrate becomes electrically thicker, more surface wave modes can exist.

Surface waves take up some part of the signal energy, thus decreasing the antenna efficiency η, which is defined as

$$\eta = \frac{P_r}{P_{in}} = \frac{P_r}{P_r + P_s + P_{cu} + P_{di}} = \frac{G(\theta, \phi)}{D(\theta, \phi)}, \tag{2.9}$$

where P_r is the radiated power, P_{in} is the input power[3], $G(\theta, \phi)$ is the power gain and $D(\theta, \phi)$ is the directive gain. The input power can be described as the sum of the power included in the surface waves P_s, the copper losses P_{cu} and the dielectric losses P_{di}.

[3]The input power is the net power accepted by the antenna from the connected transmitter. This definition of the efficiency does not include losses due to mismatches of impedance or polarization.

Table 2.1: Circuit and Antenna Requirements.

	Substrate Type	
Permittivity ε_r	*Thin*	*Thick*
Small		Antennas
Large	Lines and Circuits	Surface Waves

Additionally, surface waves introduce unwanted spurious coupling between the antenna elements. Surface wave effects are usually undesirable for antennas, so their excitation should be suppressed.

Circuit and Antenna Requirements

A microstrip structure can behave like a transmission line or like an antenna, and it is always a launcher of surface waves. The electromagnetic field in a transmission line remains concentrated in the close vicinity of the conductors so that only guided waves may be excited. Therefore such a circuit is printed on an electrically thin substrate of a large permittivity dielectric material so that the guided waves become predominant. Quite the opposite is required for an antenna. Here, the radiated waves are preferred and the geometry is adjusted to prevent energy concentration by guided waves below the patch. Compare this with the explanation of the radiation mechanism in Section 2.2.2, where the fringing fields have been determined as the primary source of radiation. Radiated waves become predominant when the substrate is electrically thick and has a low permittivity.

Finally, surface waves become significant when the substrate is electrically thick and has a large permittivity. Therefore electrically thick *and* high–permittivity substrates should not be used. In fact, the excitation of higher order modes (TE_1 and so on) should be avoided by using not too thick substrates since this would decrease the efficiency rapidly [26].

Table 2.1 shows that the requirements for circuits and antennas are contradictory. It is not possible to realize an efficient patch antenna and a non–radiating microstrip line on the same substrate. This fact will be important in the discussion of the feeding (excitation) techniques.

2.2.5 Excitation Techniques

There are a lot of different feeding techniques, but I will discuss only the most important ones.

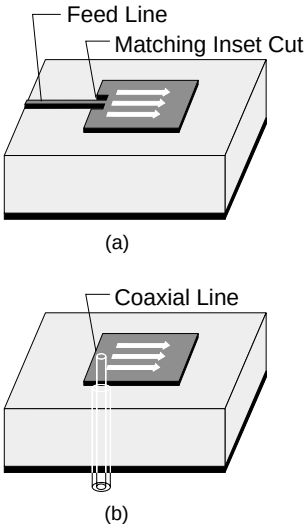

Figure 2.6: Excitation techniques: (a) Direct feed, (b) Coaxial feed.

Transmission Line Feed

The simplest way to feed a microstrip patch is to connect a microstrip line directly to the end of the patch (see Figure 2.6 (a)). This technique is also called *direct feed*. The major advantage of this technique is its simplicity in terms of fabrication and analysis. The impedance matching can be obtained by selecting the proper inset cut length.

As noted in the previous section, a microstrip structure with the transmission line and the patch at the same substrate level cannot be optimized simultaneously as an antenna *and* as a transmission line, because the specific requirements are contradictory. So a compromise has to be made and this leads to an increased spurious radiation due to the feed line. The unwanted spurious radiation means higher sidelobes and higher a cross–polarization level. In addition, with this configuration surface waves can be launched easier.

Coaxial Feed

Another way to feed the patch is by means of a coaxial line that penetrates the ground plane and the substrate (see Figure 2.6 (b)) and is then connected to the patch. The input impedance depends on the position of the feed. Therefore the antenna is matched by choosing the proper feed position. In this structure the radiator and the feeding system are shielded by the ground plane. The dielectric substrate can now be selected independently to optimize both the microstrip patch and the feeding circuit.

A drawback of this configuration is the remarkable probe loading. This means that the probe acts like an additional (and of course unwanted) reactance at the feeding

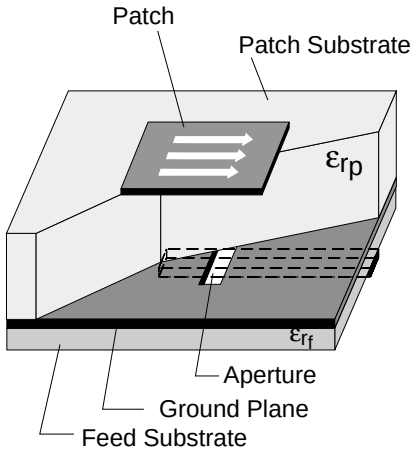

Figure 2.7: Aperture–coupled patch antenna (with part of the patch substrate removed).

point. One can easily explain this by imaging the field distortion under the patch due to the coaxial line.

Aperture Coupling

A structure that avoids a direct connection between the patch and the feed line is the aperture–coupled antenna. Here the feed consists of an open–ended microstrip line that is located on a second dielectric slab below the ground plane. The microstrip patch is residing on a separate dielectric slab above the ground plane. The two structures are electromagnetically coupled through an electrically narrow slot in the ground plane between them (see Figure 2.7). This slot is also called aperture. Note that this slot will not — or must not — resonate within the operating frequency band of the antenna because this would produce radiation towards the back of the antenna.

The radiator is shielded from the feed structure due to the ground plane. Nevertheless there is small spurious radiation caused by the feed line and coupled through the slot. Another important advantage of this structure is the freedom of selecting two different substrates. In Section 2.2.4 the contradictory requirements on the patch and feeding substrates are stated. Now, the substrate for the feed line *and* the substrate for the radiating patch can be optimized simultaneously and the issue of contradictoriness is by–passed. We will also see in Section 2.2.6 that the selection of a thick low–permittivity substrate is strictly necessary to obtain a broadband microstrip antenna. A drawback of this excitation technique is the required multilayer fabrication, which increases the production cost.

2.2.6 Bandwidth and Efficiency

A general law for antennas states that the lowest achievable quality factor of an antenna is inversely related to the antenna volume (see for example [11]). This implies that the absolute bandwidth increases with increasing patch substrate height, since the bandwidth is in inverse proportion to the quality factor.

Another important substrate parameter that influences the bandwidth is the permittivity. Here the statement is that the absolute bandwidth of a patch antenna increases with decreasing substrate permittivity.

Splitt, for example, reports in his dissertation [26] the variation of the bandwidth of an electromagnetically coupled[4] antenna over the substrate parameters H_{r_p} and ε_{r_p} (see page 97). There he finds a bandwidth that increases approximately linear with the antenna thickness for a relative permittivity of 1.1. For a thickness of $0.07\lambda_{eff}$, which I will later use as the substrate thickness, Splitt obtains a relative bandwidth of approximately 9%.

In contrast to the bandwidth, the efficiency of a patch antenna decreases with increasing substrate height. And the efficiency increases with decreasing relative permittivity. Nevertheless a relatively high efficiency in the order of 95% is predicted for a substrate with $\varepsilon_{r_p} = 1.1$ and $H_{r_p} = 0.07\lambda_{eff}$.

The low permittivity of the patch substrate is an essential property of the in the following used structure. Due to this fact, one can obtain a *broadband* and *high efficiency* microstrip antenna.

Finally I want to state that the patch width has a similar influence on the bandwidth like the substrate thickness. This comes from the fact that by increasing one of these parameters the volume of the antenna is increased.

2.3 The SSFIP Principle

The previous chapters tried to smooth the way for the introduction of the SSFIP structure. SSFIP stands for **S***trip*–**S***lot*–**F***oam*–**I***nverted* **P***atch* antenna and describes a technique to obtain broadband microstrip patch antennas. The concept was introduced by Jean François Zürcher in 1988 [32].

The SSFIP antenna presents significant advantages over standard microstrip antennas in terms of bandwidth, efficiency, cross–polarization level, weight, and cost. They shall be explained in the next section.

[4] An electromagnetically coupled patch antenna is similar to an aperture coupled antenna, just without the ground plane and the aperture. This type of antenna holds on one side of the substrate — and there is only one substrate — the feed line and on the other side the patch. Although such an antenna behaves in many ways different to the aperture–coupled one, the order of the bandwidth will be the same for both types of antenna.

2.3.1 Description of the Structure

As already pointed out in the previous sections, the patch substrate of a broadband aperture–coupled antenna needs to be thick and has a low permittivity (see Section 2.2.6 and compare to Table 2.1). Ideally, the dielectric substrate should then be air with $\varepsilon_r = 1$. Since the structure would need another support to hold the patch, the most convenient materials are hard foams. Fortunately there are foams available with a relative permittivity lower than 1.1 — as the here used *Rohacell* (for detailed informations see [14]).

Surface waves are due to the low permittivity not significantly excited on foam materials. Such foams have also a very low weight because they are mostly made of air. When a foam material is assembled in a 'sandwich' form, the result is an extremely lightweight and environmentally resistant structure.

Since foams do not present a flat, well–defined surface, they cannot be used as the base material for the metal patch. Therefore an additional dielectric slab on the top of the foam is introduced that carries the patch. This substrate is put upside–down on the foam (see Figure 2.8) to take an additional advantage from the — so called — *inverted patch*. It now serves as a protection against environmental effects, and is therefore also called radome. To have negligible effects on the antenna characteristics due to the radome, a very thin substrate is used. But it must be thick enough to be mechanically sturdily.

Since foam materials are porous, consisting mostly of minuscule air pockets, they tend to absorb moisture. The thin radome also provides protection against this absorption.

The SSFIP antenna is excited by an aperture–coupled feed, which was already discussed in the previous chapter.

2.3.2 Reflector

The SSFIP structure is improved by adding an additional metal plane below the antenna to reduce the back radiation (see Figure 2.8). The — so called — reflector is mounted with a spacing of a quarter of the free–space wavelength below the source of the back radiation. This source is the aperture.

The function of the reflector can be explained with the image theorem and array theory. First of all we assume the reflector as an infinite metal plane. This means that no back radiation exists anymore, which is (of course) a theoretical statement (because in reality it is impossible to realize an infinite reflector plane).

The reflector has also an influence on the radiation pattern in forward direction ($\theta = 0°$) and this will be analyzed in the following. By removing the reflector plane we have to add a virtual image of the antenna at exact the same distance behind the plane (Not the ground plane, but the reflector plane!). Due to the image theorem this virtual antenna is excited out–of–phase (180°) compared to the actual antenna. By choosing

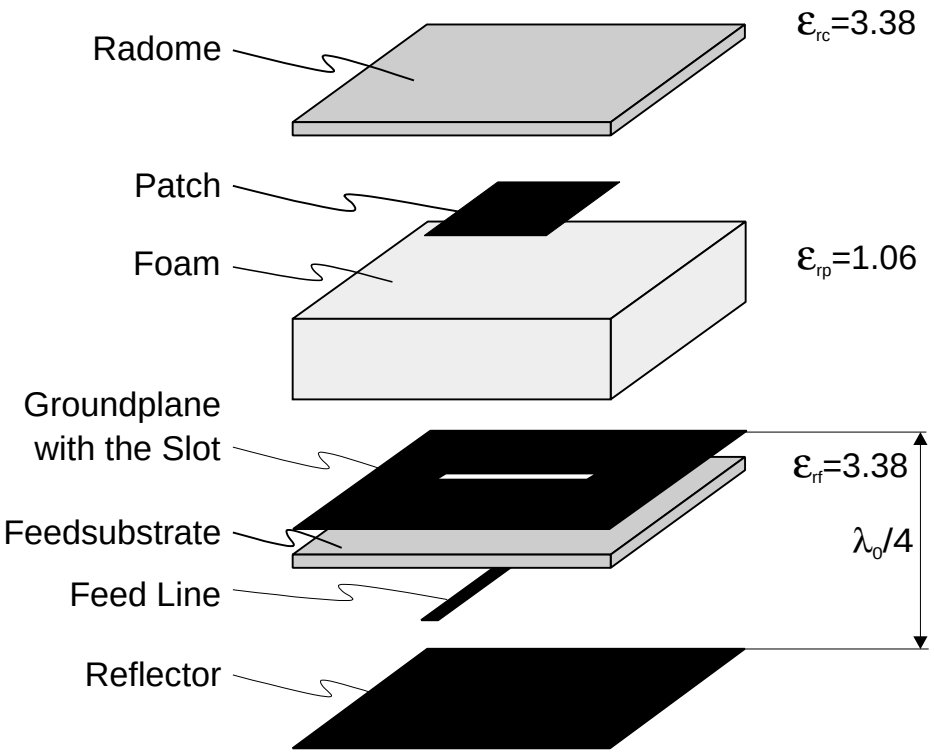

Figure 2.8: Strip–slot–foam–inverted patch antenna (exploded view). ε_{r_c}, ε_{r_p} and ε_{r_f} are the relative permittivity of the cover, the patch and the feeding substrate.

a spacing between the antenna and the reflector of $\lambda_0/4$[5] the field is constructively superposed in forward direction. With a smaller spacing the far–field would tend to cancel out and from a larger spacing more mainlobes (with directions $\theta_{max} \neq 0°$) would emerge. Both effects are of course unwanted.

Due to the infinite reflector plane the following normalized field pattern $F_a(\theta)$ arises [3]:

$$F_a(\theta) = \begin{cases} \dfrac{\sin\left(\pi - \frac{2\pi d_{refl}}{\lambda_0}\cos\theta\right)}{2\sin\left(\pi/2 - \frac{\pi d_{refl}}{\lambda_0}\cos\theta\right)} & : \quad \mid\theta\mid \leq \frac{\pi}{2} \\ 0 & : \quad \frac{\pi}{2} < \mid\theta\mid \leq \pi \end{cases} \tag{2.10}$$

where $d_{refl} = 0.5\lambda_0$.

The result is plotted in Figure 2.9. Again, there is no back radiation. Note that the assumption of an infinite reflector plane is of course unrealistic. Therefore the implemented antenna will show a certain amount of back radiation.

[5] Of course any multiple of $\lambda_0/4$ is also possible, but would result in additional unwanted sidelobes, and a larger antenna structure.

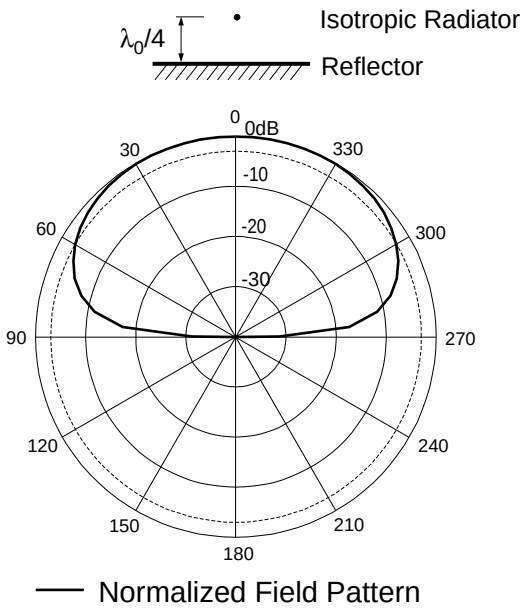

Figure 2.9: Normalized power pattern of an isotropic radiator and a reflector spaced $\lambda_0/4$ apart.

The simulation tool used for the design of the antenna is not able to account for a reflector below the structure (see Chapter 3). Therefore the influence of the reflector on the antenna pattern was introduced by simply multiplying the simulated normalized power pattern with the reflector power pattern obtained from Equation 2.10. A question that is still open is the changed directivity. The new directivity could be calculated via the equivalent solid angle, when the normalized power pattern is given for the whole sphere. This data could not be exported easily from the simulation tool and therefore the change in directivity due to the reflector could not be calculated.

2.4 Equivalent Circuit and Design Rules

For an antenna engineer it is important to understand the behaviour of an antenna. He needs to know answers to the following questions: *On which design parameter do I have to screw to change the antenna performance*, and *how do I have to change a specific design parameter to obtain the required antenna performance?*

Since an aperture–coupled antenna is a very complex electromagnetic structure, it is not possible to answer these questions at all. But, for some of the design parameters simple explanations can be given about their approximate influence on the antenna performance.

Before I do this, I will discuss an equivalent circuit for an aperture–coupled mi-

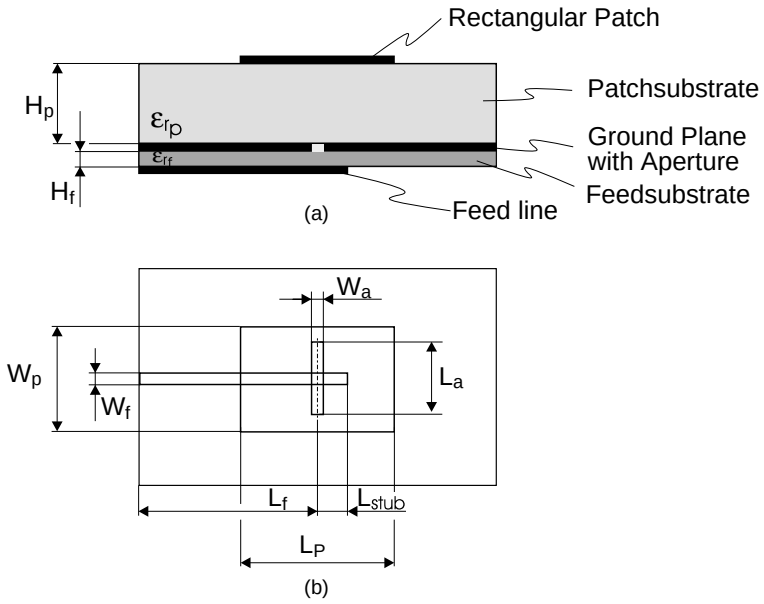

Figure 2.10: Geometry of the aperture–coupled microstrip antenna. (a) Side view. (b) Top view.

crostrip antenna that was derived by Allan Østergaard and his colleagues [19]. For my opinion this model gives some basic instructions that are crucial for the understanding of the structure.

2.4.1 Equivalent Circuit

For the development of a basic topology for the equivalent circuit examine the SSFIP structure in Figure 2.3.

Starting at the antenna input, we first look at the microstrip feed line. Away from the aperture, the feed line is well modeled by a transmission line with a characteristic impedance of $Z_{0,f}$. At one end the input port[6] of the antenna is connected, the other end is left open. Note that the feed line does not terminate exactly below the aperture. Instead, it is extended by the so called stub length L_{stub} (see Figure 2.10). In the following we will see that the stub length has a remarkable influence on the input impedance of the antenna.

At first glance we regard the coupling between the feed line and the aperture as a general three port and the aperture itself as a general two port. Look at Figure 2.11, where the patch is finally viewed as a general one port.

[6]Whenever I am talking about the input impedance or the input reflection coefficient, I take the input port of the antenna as the reference point for these two parameters.

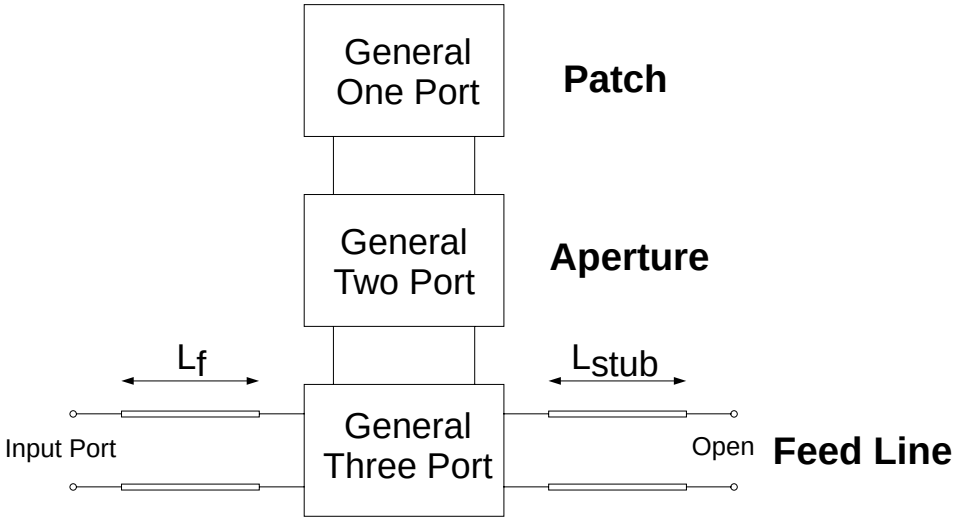

Figure 2.11: General network model for an aperture–coupled microstrip antenna.

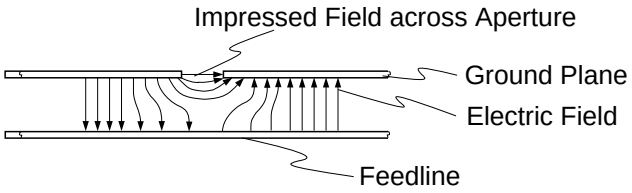

Figure 2.12: Scattering from the aperture.

Let us now try to understand the nature of the coupling between the feed line and the aperture. We do this by considering the scattering from the aperture. Figure 2.12 shows that the electric field in the aperture is predominantly directed across the aperture. The scattering off the aperture is therefore antisymmterical. From this we conclude that the coupling of the aperture can be modeled by a series connection.

The aperture itself can be regarded as a parallel tank circuit with a inductance L_{ap} and a capacitance C_{ap}. This is due to the resonant behaviour of a half wavelength aperture. But when the aperture is smaller — and this is the usual case — it behaves inductive.

Finally we take a look at the patch: As already mentioned, it can be viewed as an open–ended transmission line. To account for the fringing field at each open end a capacity C_{fring} and a resistor R_{rad} is attached. The resistors model the radiation from the patch. Instead of modeling the patch with a transmission line, it can also be

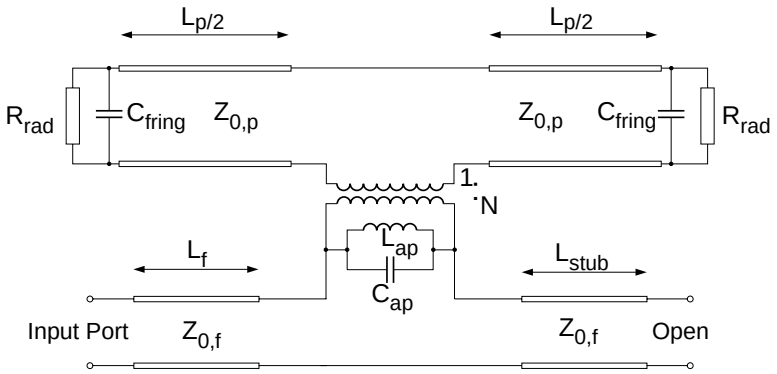

Figure 2.13: Final equivalent circuit for an aperture–coupled microstrip antenna.

viewed as a series circuit[7].

The characteristic impedance of the transmission line that models the patch $Z_{0,p}$ is of course different from $Z_{0,f}$. To transform the impedance level between the aperture and the patch transmission line a transformer is included. The transformer is placed between the aperture and the patch and has a turn ratio of N.

The result of this investigation is the equivalent circuit shown in Figure 2.13. I will not take a too deep look into the details of this model, since I use it more for understanding purposes than for calculations. But, I want to note that Østergaard and his colleagues used their results in connection with *Moment Method*–based calculations to get a powerful simulation tool.

The following chapters will give the basic information about the influence of the design parameters on the performance parameters. They will not give you quantitative advice, but a more qualitative background to give enough information to design an aperture–coupled antenna. In the following the substrate parameters will be fixed, since they have been already discussed in the preceding sections.

2.4.2 Center Frequency

The center frequency of the aperture–coupled patch is mainly controlled by the relative permittivity of the patch substrate and the length of the patch. While Equation 2.1 accounts for the fringing field, it does not account for any other influence due to the structure. But from the equivalent circuit you can see that the aperture has an influence on the resonant frequency of the antenna.

As mentioned above, the aperture usually behaves like an inductance and therefore the resonant frequency is shifted downwards[8].

[7] Why a series and not a parallel circuit? Because the open end — that equals a parallel circuit — is via the quarter–wave transformer converted into a short circuit. And the short circuit behaves like a series circuit.

[8] Imagine a series circuit with a parallel inductance and analyze the shift of resonant frequency

The inductance of the aperture increases with increasing slot dimensions – the aperture length L_a and the aperture width W_a. And so the frequency shift is larger, when the slot dimensions are increased.

Another parameter that has a rather small impact on the resonant frequency is the patch width W_p. The resonant frequency increases slightly with the patch width.

2.4.3 Coupling

During the design of this antenna array the coupling between the feed line and the patch turned out to be a more restrictive performance parameter than the impedance matching. This will be explained in Chapter 4, when the actual design is performed. Here I just want to focus on the coupling.

Although there is no clear quantitative definition of the coupling, you can help yourself with the Smith chart. A typical locus of the input impedance of a matched aperture–coupled antenna looks like a slope that crosses the abscissa near the matching point (see Figure 4.1). The coupling factor is now proportional to the radius of the slope, when simultaneously the current distribution below the slot stays at its maximum. When the radius of the slope approaches the outer circle of the Smith chart, one may think of the largest coupling factor. This is of course not true, because a fully decoupled patch would also show up with such a locus at the outer circle. Therefore I added the condition *"when simultaneously the current distribution below the slot stays at its maximum"*. From another point of view you can also say that the relation between the coupling factor and the radius is only convenient for slopes that tend to approach the center of the Smith chart. Please understand this as a help to design such an antenna. You will not find such statements in the literature, since this behaviour is up to now not fully explained by theory. Nevertheless, this procedure results from my experience during the design of the antenna.

Because of this vague definition the coupling factor can not be quantified. But you can see whether the radius of the slope changes when you modify a design parameter.

In the Smith chart you can also find the connection between the impedance matching and the coupling. When the radius of the locus changes, the input resistance near resonance is also modified. Or in other words, the impedance match can be obtained by forcing the 'right' coupling factor, which equals the 'right' resistance. Finally you just have to tune the antenna, for example by modifying the patch length, to the proper resonant frequency.

Again, I want to point out that in most theoretical papers the emphasis is on the impedance match. But for the design of an aperture–coupled microstrip antenna that fulfills the requirements stated in Chapter 1, the approach that I have outlined in the previous paragraph seems more convenient — at least in my opinion.

Back to the parameters which influence the coupling factor: Two parameters having a strong influence on the coupling are the slot length L_s and the slot width W_s. The

(with/without the parallel inductance).

coupling is increased with the slot area. This is not surprising; imagine a slot that decreases more and more and finally vanishes completely. Of course the coupling will simultaneously decrease until the patch and the feed line are fully decoupled. The slot may not be made too long, because then it may start to resonate too. This is a highly unwanted state — although it maybe increases the bandwidth (due to the second resonance) — because it strongly increases the back radiation.

Another design parameter that has a rather strong effect on the coupling factor is the stub length L_{stub}. When all other design parameters are kept constant a specific stub length leads to the maximum coupling factor. Now the question is: *How can I find the maximum easily?*

In theory [21] you find that the dominant coupling mechanism for a centered (over the aperture) patch is the magnetic dipole coupling effect — but with the assumption of an infinitely long feed line. In many other publications (see for example [22] and [30]) you find that a stub length of approximately a quarter wavelength is appropriate to match the antenna. I do agree with this statement, but want to add that this stub length does not yield an optimum coupling factor. The maximum coupling can be obtained with a stub length smaller than a quarter wavelength.

To find this stub length it is helpful to observe the current distribution on the feed line below the patch. Then you have to find the smallest stub length that lets the current — at the resonant frequency[9] — in the vicinity of the aperture stays at a maximum, because maximum current means maximum magnetic dipole coupling.

Note that I wrote some lines before "...the *dominant* coupling mechanism ...is the magnetic dipole coupling". This does not mean that scientists think that the electric dipole coupling has no contribution. Especially for the situation with very small stub lengths the question of coupling mechanisms is not fully answered. Therefore the above mentioned procedure shall more or less be understood as some hints to find the optimum configuration with the simulation tool.

Finally one sentence about the location of the patch over the aperture: The largest coupling factor can be obtained, when the patch is centered over the aperture.

A last parameter that influences the coupling is the patch width. The coupling factor can be decreased slightly, when the patch width is increased.

Exemplary quantitative results of investigations about the influence of the herein discussed parameters can be found in [22], [13], [27] and [30].

[9] A resonant frequency is a frequency at which the input impedance of the antenna is nonreactive [4].

Chapter 3

Simulation

The selection of a proper simulation tool is a crucial task in the process of the realization of printed antennas. After scanning the market for a tool that is low–priced and applicable for printed structures, I decided to use the program MultiStrip.

3.1 MultiStrip

MultiStrip is a simulation tool based on the method of moments (MoM) that was written by Prof. Splitt[1]. The simulation machine can be attributed to the group of integral equation techniques in the space and time domain. These techniques use integral equations that are derived from Maxwell's equations by applying the proper boundary conditions. Since integrals give global information — in comparison to differential equations that give local information — about the electric properties, they try to minimize a global error by applying the MoM (in this case in conjunction with Galerkins method, where the base– and the test–functions are the same). Integral techniques can be further subdivided in the classes using homogeneous or inhomogeneous Greens–functions. The application of homogeneous Greens–functions is a more general way to solve electromagnetic problems and can therefore cope with a larger class of problems. But this advantage has to be paid with an increased computational load. In opposite to this, the application of inhomogeneous Greens–functions focus on a subclass of problems (in our case the program can analyze homogeneous stratified dielectric layers), but means also a decreased computational effort. One main feature of the program is the optimization in terms of run–time and so MultiStrip can also work on an IBM–compatible PC. MultiStrip can analyze multilayered (up to three layers) microstrip antennas on multiple (up to four layers) homogeneous dielectric layers [28]. It is also possible to calculate electrodynamically and slot coupled structures, which makes the program suitable for the here designed antenna.

[1]Prof. Dr. Georg Splitt, Fachhochschule Kiel, Institut für Nachrichtentechnik und Elektronik, Legienstraße 35, 24103 Kiel, Germany.

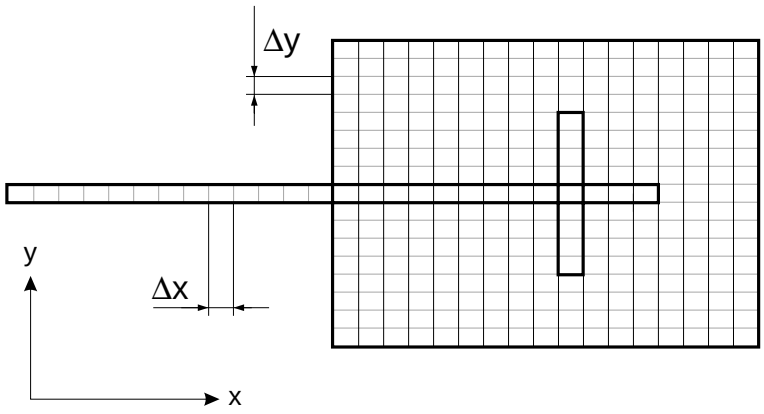

Figure 3.1: Discretization of the microstrip structure.

Due to the realized simulation method, the program accounts for all relevant effects like radiation, surface wave propagation in the substrate and dielectric losses. Also the coupling between neighbouring structures is calculated, although with some restrictions.

3.2 Experiences with MultiStrip

The design of the antenna was mainly based on the reliable simulation results that have been obtained with MultiStrip. In the Chapters 4 and 5 you will find the excellent agreement between simulation results and measurements.

Nevertheless there are some restrictions and disadvantages that influence the work with MultiStrip considerably.

First of all the low versatility in terms of discretization: The structure has to be divided into equi–sized rectangles (see Figure 3.1). This means that in connection with aperture–coupling the program only allows to lay a homogeneous grid over the structure. Therefore you have to define the segmentation size in x– and y–direction by parameters Δx and Δy. The grid dimension must meet the following conditions:

$$\Delta x, \Delta y \approx \frac{1}{20}\lambda_{eff} \quad \text{or smaller}$$

and

$$\Delta x/\Delta y \approx 1.$$

For my design it meant $\Delta x, \Delta y \approx 4mm$. With the selection of the segment size you also define the smallest possible geometry factors. In this application for example the feed line width has to be near $2mm$. Therefore I had to choose $\Delta y = 2mm$,

which means that I simulated the structure with an unnecessary high resolution. A similar situation occurs in the x–direction with the slot width. This causes increased simulation run–time.

The advantage of such a fine discretization is that you can vary the parameters in smaller steps. Nevertheless, some parameters are very sensitive (for example the patch length influences the resonant frequency) and should therefore be changed in even tinyer steps. The work–around here is to focus on a specific performance parameter and more or less don't worry about the others[2]. For example, I optimized the coupling between the feed line and the patch by varying the stub length (in x–direction). To change the stub length in tiny steps (by changing Δx and the number of segments that describe the stub length) I also altered the patch length and therefore shifted the resonant frequency — which I did not take care about. The resonant frequency again was then optimized in a similar way. As you can see from this procedure, especially the optimization of the array, where the slot showed a larger complexity, took a lot of time.

The second restriction is in terms of coupling capabilities. MultiStrip can only calculate the coupling within a certain radius (currently the maximum radius is $60\Delta x$ and $60\Delta y$, which equals in my case approximately λ_0). Therefore the mutual coupling in an array with more than three elements can not be calculated accurately.

Because of the time–consuming simulations, I decided to optimze only the single element for the array design. Additionally I computed the coupling between two neighbouring antenna elements (in a three element array) from time to time to check the mutual coupling. From the results presented in Chapter 5 you will see that MultiStrip predicts — despite the restricted coupling capability — the maximum mutual coupling very accurately.

3.3 Ensemble

From Richard Hall[3] I fortunately got an invitation to get the final antenna array simulated by BMT's simulation tool Ensemble.

Ensemble is also a MoM based CAD tool that works with integral equations in the frequency domain. The program comprises an automatic mesh generator that uses rectangular and triangular segments. So there are no restrictions in terms of antenna geometry. Ensemble (Version 4.0) can calculate structures consisting of nine dielectric layers, five metal layers and up to two ground planes. Therefore it is even possible to simulate an aperture–coupled microstrip antenna with stacked patches. Because of the versatile features of the program, the whole antenna array — with the exception of the

[2] Actually you work with the idea that the other performance parameters are independent from the one that is just focused — which is of course not fully true.

[3] Richard C. Hall, Ph. D., is a Senior Member of Technical Staff at Boulder Microwave Technologies (BMT), Inc. 2336 Canyon Blvd., Suite 102, Boulder, CO 80302 USA. He is still engaged in the improvement of the simulation machine of Ensemble.

finite reflector plane — could be analyzed. Even the adhesive tape layers could have been introduced in the simulation.

As already mentioned only the final antenna array has been calculated with Ensemble, and the results are presented is Chapter 5.

Chapter 4

Single Element Antenna

After getting familiar with MultiStrip, the next step was to get a feeling for the microstrip patch structure. From theory it is well known that the substrate plays a key–role in the design of such an antenna. Therefore the first task was to select proper substrate materials.

The next step was to find out how strong the design parameters actually influence the performance of the antenna. Combining this information with the requirements for the antenna, I found the — for this design — most sensible and important design parameters.

Equipped with this knowledge I started to design the first single patch antenna. The antenna had to fulfill the requirements stated in Chapter 1. The design process, the implementation, and the results are reported in the sequel.

4.1 Substrate Materials

The aperture coupled patch antenna consists of three — not necessarily different — substrate materials. The selection of these materials is discussed in the following.

4.1.1 Patch Substrate

The key–question of the design was probably the question of the patch substrate material. As I have already stated in Section 2.2.6 and Section 2.3, the patch substrate has to be a foam material. With such a low–permittivity substrate the implementation of a *broadband* microstrip antenna is possible.

From different publications (for example [25], [33]) and also from personal contacts with other researchers I got known of the foam material *Rohacell*[1]. Rohacell is a closed–cell rigid foam plastic based on PMI (**P**oly**m**ethacryl**i**mid) with a very fine cell

[1] *Rohacell* is produced by *Röhm GmbH*, Chemische Fabrik, Kirschenallee, D – 64293 Darmstadt. The material is distributed in Austria by *Ferdinand Thun–Hohenstein GmbH*, Lamezanstraße 17, A – 1231 Wien, Austria.

Table 4.1: Technical properties of Rohacell HF 51.

Property	*Unit*	*Rohacell HF 51*
Relative Permittivity [a]	1	1.057
Loss Tangent	1	$< 2{\cdot}10^{-4}$
Density	kg/m^3	32
Heat Distortion Temperature	$°C$	180

[a] The permittivity is reported for 2.5GHz. Note, that there is no measuring error stated.

structure (for further details see [14]). There is a specific quality for high–frequency applications available that is called *Rohacell HF 51*. The most important technical parameters of Rohacell HF 51 are listed in Table 4.1.

Concerning the bonding properties, Rohacell HF is suitable for bonding with all reaction adhesive systems. There is only little distortion of the electrical parameters due to absorption of moisture, because the water–molecules cannot oscillate. But by using an additional protective layer that is impermeable for water, the antenna can operate in any humid environment without distortion.

Although I have selected a specific substrate, I did not specify the substrate height yet. We saw in Section 2.2.6 that the bandwidth increases with the thickness of the substrate. But, as already discussed in Section 2.4.3, the coupling decreases with increasing substrate thickness. So I had to choose a substrate thickness that is large enough to fulfill the bandwidth requirements and that is small enough to realize a proper coupling. I started simulations with a thickness of 4mm. Soon I found out that this thickness was too small to meet the bandwidth requirements. In the following I therefore used thicker substrates. For the discussion of the single element I implemented an antenna with a $6.6mm$ substrate[2]. While for the design of the array I used a substrate height of $8.1mm$.

4.1.2 Feed Substrate

The purpose of the feed line is to carry energy from a connector to the actual antenna — and so to launch guided waves only. From Section 2.2.4 we know that an electrically thin substrate with large permittivity is therefore suitable. Another fact that influenced the selection of the feed substrate is the width of the feed line. From Equation 2.5 you can see that the characteristic impedance of a microstrip line depends only on the normalized line width W/H, and not on the absolute value of W. This implies that for a smaller substrate height a corresponding smaller line width has to be used to obtain the same characteristic impedance. And from this equation we also see that when a

[2] The uncertainty of the thickness is in the order of $0.1mm$.

Table 4.2: Technical properties of $RO4003^{TM}$.

Property	*Unit*	$RO4003^{TM}$
Relative Permittivity [a]	1	3.38 ± 0.05
Thickness	mm	0.81 ± 0.04
Dissipation Factor	1	$< 2{\cdot}10^{-3}$
Heat Distortion Temperature	$°C$	280

[a] The permittivity is reported for a frequency up to 10GHz.

larger relative permittivity is used, the normalized line width has to be decreased to obtain a constant impedance level.

So the substrate parameters have to be selected in a way that a convenient line width for a 50Ω–line is obtained. Together with the results from Section 4.4.1 I chose the following substrate material:

$RO4003^{TM}$[3] with $\varepsilon_r = 3.38$ and a substrate height of $0.8mm$. $RO4003^{TM}$ is a woven glass reinforced, ceramic filled material that was developed to provide high frequency performance comparable to woven glass PTFE substrates for reasonable prices. Some more technical parameters can be found in Table 4.2.

4.1.3 Cover Substrate

At last, the dielectric material for the radome has to be specified. For convenience I also used $RO4003^{TM}$, because it is available with a very small height of 0.2 ± 0.03mm. This small height is important, since the radome will then alter the performance of the antenna insignificantly. In this context I want to note that $RO4003^{TM}$ has a very low — but non–zero — water absorption. So if you want to make the antenna fully uninfluenced by the environmental humidity, the radome has to be covered with a water resistant layer.

4.2 Connectors

The microstrip antenna is connected to the outside (transceiver, measuring instrument) by means of microstrip–to–coaxial line transitions. The engineer has to select a transition that is well–fitting to the input feed line to avoid disturbances of the electrical field configuration — or avoid sharp discontinuities.

[3] $RO4003^{TM}$ is a trademark of Rogers Co. It is distributed in Europe by Rogers–Mektron, B – 9000 Gent, Belgium.

Therefore I used a stripline SMA connector[4] from Rosenberger[5] as the transition device (for further details see [12]). The centerconductor is a microstrip line with 1.3mm width, and this has to be soldered to the feed line. As you will see in Section 4.4.1 the feed line has a width of approximately $1.9mm$, so there is no significant discontinuity and therefore no taper is required.

To cause possible low influence on the radiation pattern of the antenna a connector type with a small flange was selected. Such disturbances come from the fact that the flange is grounded and so carries a current that may be an unwanted source for radiation.

Note that the connector has effects on the measured input phase, due to the dielectric within the connector and its finite length (see Section 4.8).

4.3 Uncertainty Analysis

An important question that arises during the design process is: *How strong do the uncertainties in the design parameters affect the performance of the antenna?* You may think that the answer of this question gets of interest only when the actual implementation takes place. But, you will see that it has a remarkable effect on the bandwidth requirements and shall therefore be treated right now. From my experience with the design and implementation of microstrip antennas the only performance parameter that has to be considered during the uncertainty analysis is the resonant frequency.

From [1] I obtain a first order change in the resonant frequency Δf_0 resulting in

$$|\Delta f_0| = \sqrt{\left(\frac{\partial f_0}{\partial L_p}\Delta L_p\right)^2 + \left(\frac{\partial f_0}{\partial \varepsilon_{eff}}\Delta \varepsilon_{eff}\right)^2}, \tag{4.1}$$

where ΔL_p is the uncertainty of the patch length due to the fabrication. And $\Delta\varepsilon_{eff}$ is the change in the effective permittivity due to the uncertainties in the relative permittivity[6], given by

$$\Delta\varepsilon_{eff} = \frac{\partial \varepsilon_{eff}}{\partial \varepsilon_{r_p}}\Delta\varepsilon_{r_p}. \tag{4.2}$$

Using Equation 4.2 in connection with Equation 2.1 and Equation 2.3[7] I obtained

[4]The precise description of the connector is SMA bulkhead receptacle with centerconductor 90° twisted and rectangular flange (RT–Code No. 32 K 703–600 D3).

[5]Rosenberger Hochfrequenztechnik, Germany.

[6]In the following equation I disregarded the insignificant influence of the uncertainties of the design parameters L_p, W_p and H_p, since I am only interested in the order of the final change in the resonant frequency and not in a very accurate result.

[7]For simplicity I neglected partly (in the expression for the factor a) the influence of the normalized width W_p/H_p and used $a = 1$.

$$\frac{|\Delta f_0|}{f_0} = \sqrt{\left(\frac{\Delta L_p}{L_p}\right)^2 + \left(\frac{1}{4}\frac{\Delta\varepsilon_{r_p}}{\varepsilon_{eff}}\left(1 + \left(1 + 10\frac{H_p}{W_p}\right)^{-b}\right)\right)^2}, \tag{4.3}$$

with

$$b = 0.564\left(\frac{\varepsilon_{r_p} - 0.9}{\varepsilon_{r_p} + 3}\right)^{0.053}.$$

With Equation 4.3 the change in resonant frequency due to the uncertainties in the patch length and in the relative permittivity of the patch substrate can be calculated. By assuming[8] $\Delta L_p = 0.1mm$, $L_p = 50mm$, $W_p = 25mm$, $H_p = 8mm$ $\varepsilon_{r_p} = 1.06$, $\varepsilon_{eff} = 1.05$ and $\Delta\varepsilon_{r_p} = 0.02$ (which equals approximately 2% of ε_{r_p}), I obtained

$$\frac{|\Delta f_0|}{f_0} = 0.74\%.$$

It is important to note that the major contribution to this frequency change comes from the uncertainty in the permittivity and not from the uncertainty in the patch length. So for a first order approximation I conclude that the Δf_0 increases linear with ε_{r_p}.

Up to now I assumed only that the uncertainties of the permittivity come from the production. Of course, if the permittivity changes due to other factors, like the humidity or the temperature, the resonant frequency would change accordingly. This already gives a hint on what the designer has to take care of: The antenna has to be shielded from any humidity that would change the permittivity of the foam significantly, and the thermal coefficient for the permittivity has to be checked.

Unfortunately I did not get any specific information about the thermal coefficient of Rohacell. Therefore I measured the resonant frequency of a patch antenna once with the substrate under normal room conditions and the second time after the substrate was dried at a temperature of approximately $80°C$ for 24 hours. The change in resonant frequency was unmeasureable.

An important conclusion from the result obtained above is that the requirement on the bandwidth of the antenna has to be rewritten: To account for the change in resonant frequency in the order of a 0.75%, the bandwidth has to be increased for twice as much — 1.5%. This comes from the fact that the resonant frequency — and with it the upper and the lower band limit — could vary in both directions.

The new bandwidth requirement is now (compare with Section 1.2.2):

RBW = 4.9% or BW = 120MHz.

[8]Some of the values stated here are already results from later investigations.

4.4 Antenna Design

In this section I will discuss the design procedure of a single element antenna.

4.4.1 Feed Line

The first step is to compute the proper feed line width W_f to obtain a 50Ω–line. This is done by taking the feed substrate parameters, $H_f = 0.81mm$ and $\varepsilon_{r_f} = 3.38$, and computing by the use of Equation 2.5 and 2.3 iteratively the proper feed line width to obtain a characteristic impedance of 50Ω. From this I got:

$$W_f = 1.88mm \quad \text{with} \quad Z_c = 49.9\Omega.$$

When you take a look at Figure 2.10 you can see that I have to specify two more parameters, L_f and L_{stub}, that give the full length of the feed line. The feed line length L_f changes only the phase[9] of the input impedance, at least when L_f is long enough. What does 'long enough' mean? The feed line has to be long enough so that the field configuration can become that of a quasi–TEM wave on a microstrip line. But due to the inevitable discontinuity in the field configuration at the input connector, the field pattern takes some $0.1\lambda_{eff_f}$ to form the typical microstrip wave configuration.

To have a certain margin I decided to use a feed line length of approximately λ_{eff_f}. With Equation 2.3 the effective permittivity is computed to

$$\varepsilon_{eff_f} = 2.68,$$

and with

$$\lambda_{eff} = \frac{\lambda_0}{\sqrt{\varepsilon_{eff}}} \tag{4.4}$$

a feed line length of $L_f \approx 74mm$ is obtained.

As above mentioned the feed line length influences the phase of the input impedance and so the locus of the input reflection coefficient in the Smith chart. The question, whether any location in the Smith chart is preferred can not be answered simply. Although some scientists mean that with the locus near the short circuit point in the Smith chart, which is equal to a lower impedance level, the matching of the antenna can be easier. I also have to state that in most publications the locus of the input reflection coefficient actually *is* near the short circuit point. For the single element antenna I finally used a feed length of $L_f = 81.2mm$.

The stub length L_{stub} will be treated in a later section.

[9] Any attenuation due to losses of the feed line will be neglected.

4.4.2 Patch Dimensions

First of all the patch length has to be computed, at least an initial value to start with the simulation. From Equation 2.1, 2.3 and the given parameters — resonant frequency $f_0 = 2.45GHz$, $\varepsilon_{r_p} = 1.06$, $H_p = 6.6mm$ and an initial value for the patch width $W_p = 40mm$ — the patch length is computed to

$$\mathrm{L}_p = 51.06mm.$$

When I simulated such an antenna with typical values for the slot dimensions (see next section), I obtained a resonant frequency of approximately $2.25GHz$. The large difference between the predicted and the simulated value is due to the influence of the slot (see Section 2.4.2). To find the right value of the patch length, the old value of $51.06mm$ has to be multiplied with the ratio of the resonant frequencies $2.25/2.45$ and so a new patch length of $L_p = 46.8mm$ is obtained. The fine tuning — again by changing the patch length slightly — of the antenna is accomplished when all other parameters are fixed.

Next I want to comment on the patch width. From theory (for example from [1]) we know that the optimum — in terms of efficiency — patch width is in the order of half of the effective wavelength in the patch substrate. This means a patch width similar to the patch length and therefore a squared patch shape. Unfortunately this patch width is too large for our purposes. This comes from the requirement that the single elements shall be spaced with a distance of $60mm$ apart (compare Section 1.2). But with a patch width in the order of $50mm$ only approximately $10mm$ remain as distance between the two non–radiating patch edges. This would result in an undesired large mutual coupling. So I have to choose a smaller patch width, here I took $W_p \approx 25mm$. The question of the patch width and its influence on other design parameters will be discussed in more details in Chapter 5.

4.4.3 Coupling

At last the proper coupling, and so the impedance matching, has to be gained. This part of the design was the most difficult task. First I selected a slot width that seemed convenient — $W_s \approx 1 \ldots 2mm$. A larger slot width would cause a decreased polarization purity, therefore a possible narrow slot is desirable. Bear in mind that I am considerably restricted in choosing the geometry due to the simulation program (see Chapter 3).

Now I tuned the slot length until a proper coupling was obtained. Figure 4.1 shows some typical loci of the input reflection coefficient for different slot lengths. You can see that the radii of the slopes increase with the slot length, which means an increased coupling (compare Section 2.4.3). Note that only the qualitative behaviour is from interest. Because the quantitative behaviour depends also on other design parameters (for example the patch width and the stub length have a rather significant influence on the coupling), a detailed analysis has to be performed anyway.

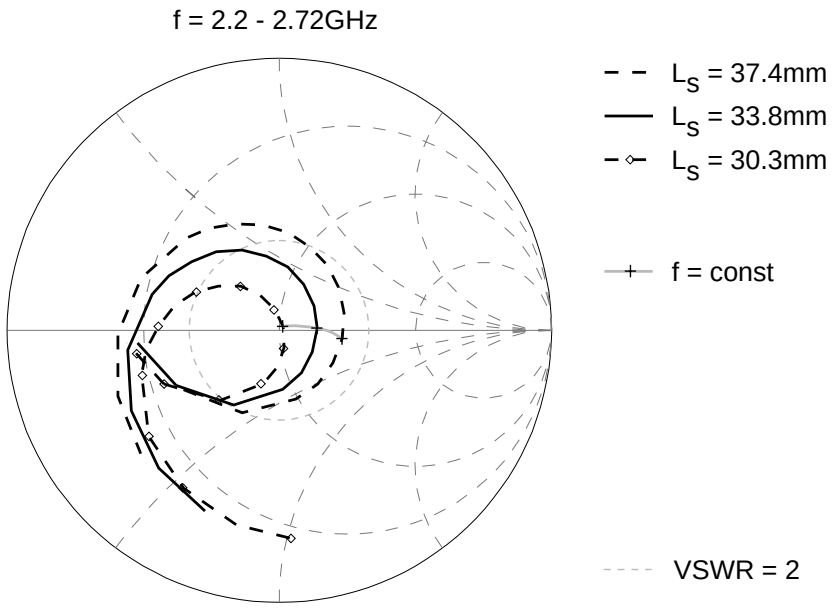

Figure 4.1: Calculated input impedance as a function of slot length.

After I have achieved a configuration that is more or less matched, I tried to find the stub length for optimum coupling. Figure 4.2 shows some loci with varied stub length. You can see that increasing the stub length decreases the coupling — and the radii of the slopes decrease. On the other side, when you choose smaller stub lengths, you observe an increased slope–radius and so an increased coupling. But when the stub length becomes very small the coupling decreases drastically with further decreasing the stub length. An explanation for this could be that when the stub length is too small the current below the slot cannot reach its maximum (at the resonant frequency). So the solution is to observe also the current distribution, when you decrease the stub length any further. You also have to check the field distribution in the slot. By observing this field you can check whether any unwanted higher order modes are excited. I also want to note that the behaviour of the phase of the different loci I have shown is not a general one. But it was experienced with the here used configurations.

4.4.4 Tuning

The last two tasks are the fine tuning of the phase and the resonant frequency. The input impedance phase is changed by varying the feed length L_f. And the input impedance can be influenced simply by screwing on the patch length L_p. The advantage of this type of frequency tuning is that the locus of the impedance stays on the same location. Only the frequency behaviour is changed, which means that the impedance

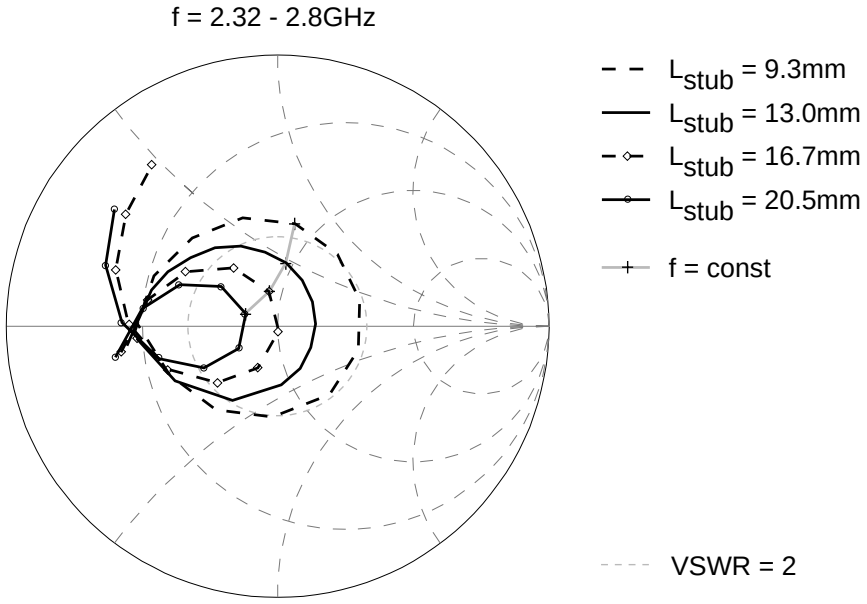

Figure 4.2: Calculated input impedance as a function of stub length.

at a specific frequency moves on the locus.

An influence factor on the resonant frequency that can not be accounted for in the simulation (MultiStrip) is the permittivity of the used adhesive tape (see Section 4.6). Therefore I used the following work–around: I increased the patch substrate height by the thickness of the two layers of the tape and further increased the relative permittivity of the patch substrate up to a value of 1.09, where the simulation predicts the resonant frequency accurately. This value was found by an experiment. I simply realized a test antenna and measured the resonant frequency with and without the cement layers. The resonant frequency was of course shifted downwards, when the tapes have been used because they had a larger permittivity than the foam substrate[10]. The measured shift of resonant frequency is approximately $20MHz$.

4.5 Simulation Result

The final design parameters and the performance of an optimized aperture–coupled patch antenna are summarized in Table 4.3 and Table 4.4, respectively.

[10]Unfortunately it was impossible to get detailed electrical parameters for the adhesive tape and therefore an experimental way had to be used.

Table 4.3: Geometry of the single element antenna.

Antenna Part	*Parameter*	*Value*
Cover Substrate	Relative Permittivity ε_{r_c}	3.38
	Height H_c	0.2mm
	Losses $\tan\delta_c$	$2{\cdot}10^{-3}$
Patch	Length L_p	46.63mm
	Width W_p	25.65mm
Patch Substrate	Relative Permittivity ε_{r_p}	1.09
	Height H_p	6.6mm
	Losses $\tan\delta_p$	$2{\cdot}10^{-4}$
Slot	Length L_s	22.23mm
	Width W_s	1.71mm
Patch Substrate	Relative Permittivity ε_{r_f}	3.38
	Height H_f	0.81mm
	Losses $\tan\delta_f$	$2{\cdot}10^{-3}$
Feed Line	Length L_f	81.21mm
	Width W_f	1.88mm
	Stub Length L_{stub}	8.32mm

4.5.1 Input Impedance and Bandwidth

Figure 4.3 shows the input impedance in the Smith chart over the frequency range from $2.2 - 2.7GHz$. It also includes a centered circle (drawn in grey) that corresponds to the reflection coefficient $\mid \rho \mid = 1/3$, which equals a voltage–standing–ratio $VSWR = 2$. The bandwidth is — as already mentioned in Chapter 1 — defined as the frequency range within the $VSWR \leq 2$[11], which means that the antenna is properly matched. Therefore the grey circle shows the limit for the bandwidth, which I will call the 'bandwidth–circle'.

Usually when you want to match an antenna you try to shift the impedance locus as near as possible to the center of the Smith chart (the matching point) to obtain a low return loss at resonant frequency. But, to obtain a large bandwidth it is required to shift a possible large part of the impedance locus inside the bandwidth–circle. And this does not mean a minimized return loss at the resonant frequency, but a smoother return loss trace over the frequency (compare Figures 4.3 and 4.4). Or, in other words, it is of course possible to minimize the return loss near the resonant frequency even more and so yield a very sharp curve trace. But this is not the aim in my design. Here I wanted to maximize the obtained bandwidth. With a patch substrate height of $6.6mm$ — which equals approximately $0.07\lambda_{eff_p}$ — a bandwidth of 153MHz was obtained.

[11] This corresponds to a return loss of $\leq -9.54dB$.

Table 4.4: Performance of the simulated single patch antenna.

Parameter		*Value*
Bandwidth		153MHz
Polarization Purity		∞
Directivity D	without reflector	8.7dBi
Efficiency η		91%
Maximum Gain G		8.3dBi
Front–to–Back Ratio F/B H–plane		18.8dB
Half–power Beamwidth H–plane		86°
-10dB Beamwidth H–plane		140°
Front–to–Back Ratio F/B E–plane		16.6dB
Half–power Beamwidth E–plane		68°
-10dB Beamwidth E–plane		122°
Directivity D	with reflector	$\approx$ 9.2dBi
Efficiency η		—
Maximum Gain G		—
Front–to–Back Ratio F/B		∞
Half–power Beamwidth H–plane		84°
-10dB Beamwidth H–plane		125°
Half–power Beamwidth E–plane		68°
-10dB Beamwidth E–plane		111°

Figure 4.4 shows the simulation result of the return loss over the same frequency range. The figure includes two curves for the return loss. The dashed line shows the return loss for a relative patch permittivity of 1.057 and the solid line shows the result for $\varepsilon_{r_p} = 1.09$. The value of 1.057 is the nominal value of the substrate permittivity, while the value of 1.09 already accounts for the influence of the tape layers. The figure also includes a shaded area that represents the ISM–band. The simulation result shows that the return loss has a nearly symmetrical trace according the center frequency. The obtained bandwidth is larger than the required bandwidth of $120MHz$. Therefore there is enough margin on both band limits to compensate for other uncertainties in the design parameters.

4.5.2 Radiation Pattern

A comparison of the normalized power pattern for the H–plane (solid line) and E–plane (dashed line) is shown in Figure 4.5. The E–plane is, as indicated in the figure by the top view of the patch antenna, the plane parallel to the feed line and the H–plane lays perpendicular to the feed line. This designation comes from the fact that the main direction of the current in the patch is parallel to the feed line — which then describes

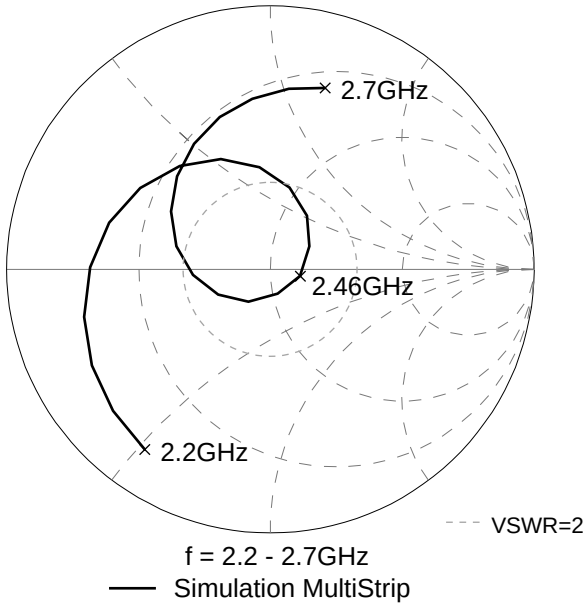

Figure 4.3: Simulation result for the input impedance of the single element antenna for a frequency range from $2.2 - 2.7GHz$.

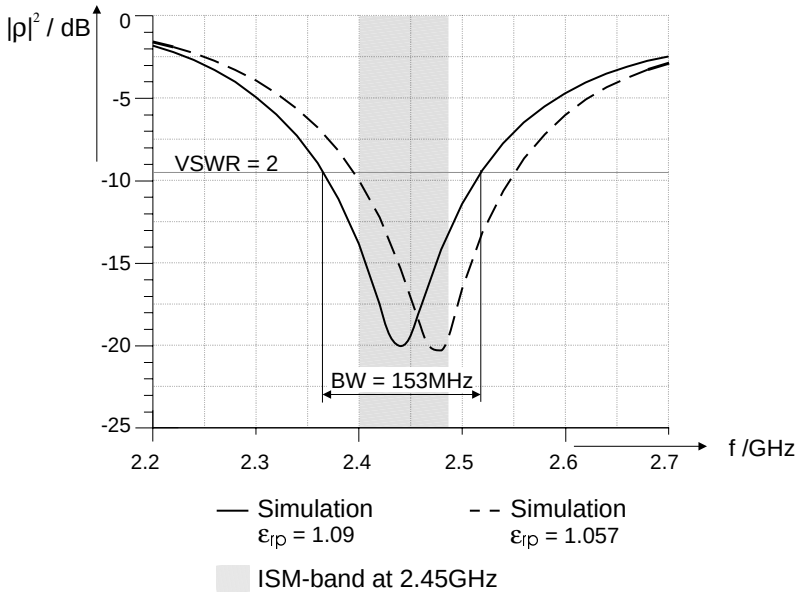

Figure 4.4: Simulation result for the return loss of the single element antenna for a frequency range from $2.2 - 2.7GHz$. The solid line shows the final result for a relative permittivity of the patch substrate of 1.09, which already accounts for the influence of the adhesive tape layers.

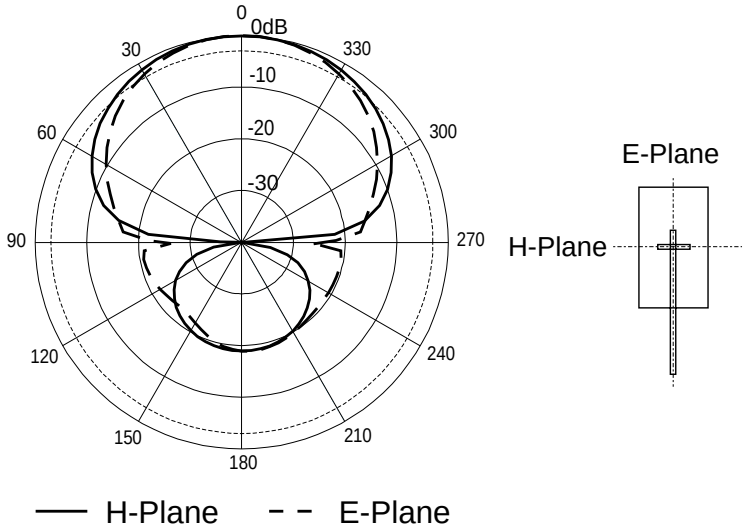

Figure 4.5: Calculated normalized vertical power pattern of the single element antenna at a frequency of 2.45GHz.

the E–plane. Note that the results in Figure 4.5 are for an aperture–coupled patch antenna *without* a reflector.

The directivity over the isotropic radiator was predicted to be $8.7dBi$, while the antenna efficiency is 91%. This results in a maximum gain over the isotropic radiator of $G = 8.7dBi - 10\log_{10}0.91 = 8.3dBi$. When you take a closer look at the two patterns, you can see that the H–plane pattern is symmetrical, while the E–plane is not. This is self–evident, since the structure shows an unsymmetry due to the feed line. We can also find a slightly narrower beamwidth in the E–plane than in the H–plane, while the back radiation is higher in the E–plane than in the H–plane.

Figure 4.6 shows the predicted radiation pattern for the antenna with (dashed line) and without (solid line) an infinitely large reflector.

You can observe that the reflector removes theoretically any back radiation, while simultaneously decreasing the beamwidth of the mainlobe. Of course the directivity is then increased. The change of the directivity could not be calculated (see Section 2.3.2), but I have tried to approximate it. What I can calculate is the directivity of an antenna with the same vertical pattern as for example the E–plane pattern of the patch antenna,; when I assume a rotation–symmetrical antenna pattern[12]:

$$D = \frac{U_{max}}{U_{ave}}, \tag{4.5}$$

where U_{max} and U_{ave} are the maximum and average radiation intensity in the E–plane, respectively. These two values can be easily derived from the simulation data. I

[12]This is of course not true for this structure, but be aware that there is only a slight difference between the E– and H–plane pattern.

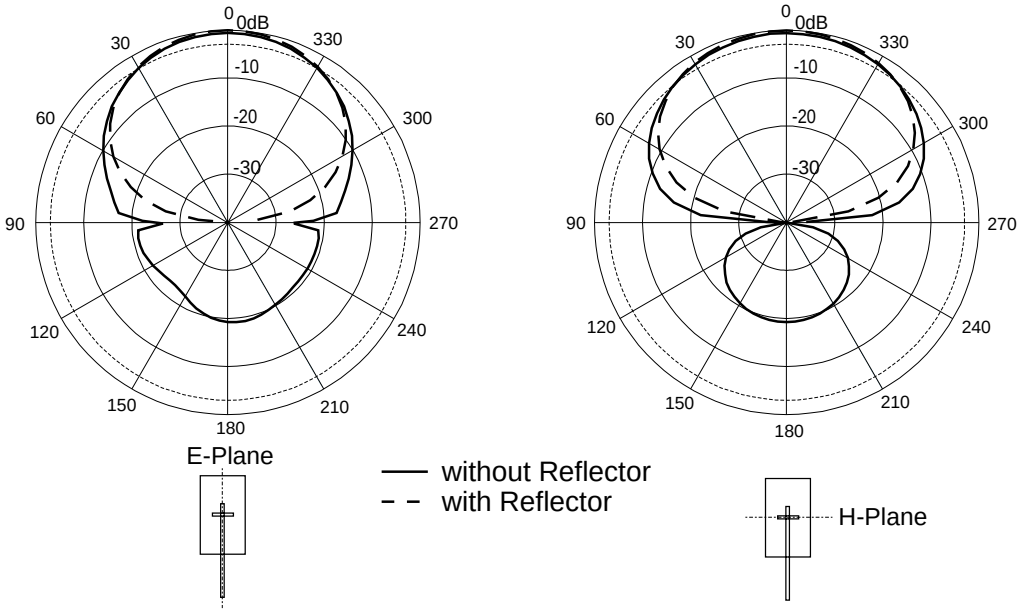

Figure 4.6: Calculated vertical radiation pattern of the single element antenna at a frequency of 2.45GHz with and without an infinitely large reflector.

calculated this directivity for the pattern with and without the reflector. The difference between these directivities was in the order of $0.5dB$ for both the E– and the H–plane. Figure 4.6 accounts for this fact, and therefore the pattern for the antenna with reflector has a larger directivity. But again, please note that this change in directivity is not an exact result[13].

The influence of the reflector on the gain cannot be approximated and therefore you will find no values for the gain and efficiency of the final antenna structure in Table 4.4.

Figure 4.7 shows the 3–dimensional radiation pattern for the antenna structure without the reflector. It should give you an idea of the overall radiation of such an antenna. In this figure I have not only included the co–polarization component E_{co}, but also the cross–polarization component E_{cross} and therefore the mesh of E_{co} is broken up to see E_{cross}. An interesting fact is that E_{cross} has nulls in E– and H–plane. This means a polarization purity of infinity in these planes, but smaller values elsewhere.

4.6 Implementation

To implement such an antenna a few practical problems have to resolved. The following section describes these issues.

[13]The largest increase in directivity that is achievable due to an infinite reflector plane for any type of antenna is 3dB — which is the case for the isotropic radiator. While the directivity stays the same, when an antenna has 'no' back radiation.

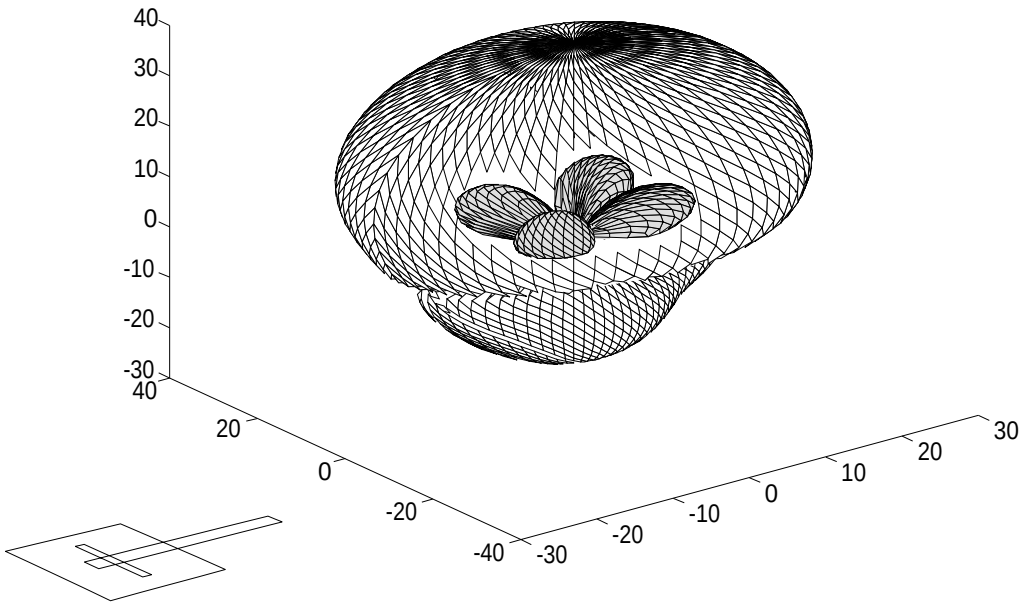

Figure 4.7: 3D–radiation pattern for the single element antenna at a frequency of 2.45GHz. The mesh for the co–polarization component (white filled) is broken up to see the cross–polarization component (grey filled). The axis give relative values of the power pattern in decibels.

4.6.1 Printed Structures

The first step was to fabricate the printed structures that the antenna consists of. The cover substrate that holds the patch, and the feed substrate that carries the ground plane with the slot and the feed line have been build by using a photo–etching process. To get the required artwork generation, I have used the software package HFCAD[14]. The achieved accuracy for the realized printed structures was in the order of 0.1mm.

4.6.2 Assembling Procedure

The antenna consists of four layers (the cover substrate, the patch — or foam — substrate, the feed substrate and the reflector plane) that have to be put together.

Adhesive Tape

The foam substrate sticks together with the cover substrate and the feed substrate. An important fact in this task is the proper alignment of all three layers, as this influences the geometrical parameters (for example the stub length) of the antenna.

[14]HFCAD is an add–on package for the software program AUTOCAD. HFCAD was realized at the INTHF.

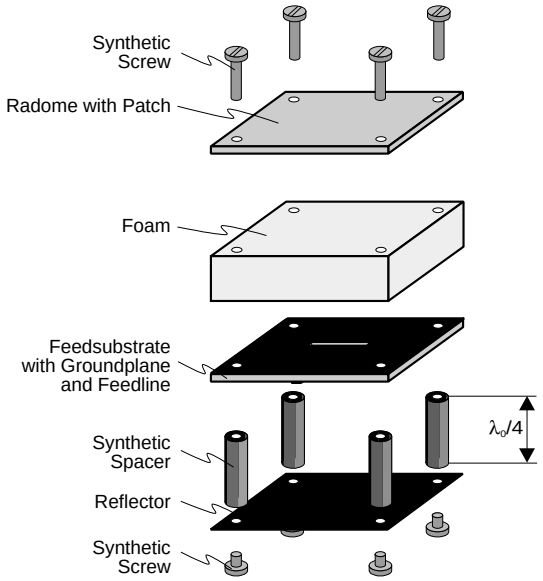

Figure 4.8: Assembling of the single element prototype.

To accomplish a proper alignment I plotted with HFCAD four drilling–marks on the artwork generation. So each layer got four holes with well defined locations. I assembled the four structures by using synthetic screws that have neglectable influence on the electric behaviour. The drill–holes are of course near the border of each layer and so possibly far away from the patch and the feed line. This procedure was used for the first prototypes. For the final construction it was also clear that the antenna should not consist of any screws. Therefore to stick the foam substrate with the other two layers a cement has to be used. I decided to use a double–sided pressure sensitive adhesive tape that is easy to handle and has a defined thickness. The tape is a product from *3M* and is called *Scotch Acrylac Foam VHB No. 4969*. It has a thickness of 0.13mm and is 25mm wide.

Mounting the Reflector

When you take a look at the antenna structure (Figure 2.3) you can see that between the feed substrate and the reflector no additional substrate is required. But to obtain the required spacing of $30mm$ I used synthetic spacers that are mounted with another four screws. In Figure 4.8 you find a sketch of a single element prototype.

4.7 Performing the Measurements

4.7.1 Input Impedance and Bandwidth

The input impedance of the antenna has been measured with a network analyzer system from HP[15] over a frequency range from 2.2 — 2.7GHz. To get reliable measurement results with the network analyzer you have to measure in a calibrated mode. Nevertheless there are still errors introduced:

The circuit is observed through a connector, because the measuring instrument has coaxial ports and cannot measure directly on the microstrip line. This causes mainly phase–shifts, which can be compensated. To do this, I took an unused connector and short–circuited the centerconductor. Then I measured the input impedance of this short–circuited connector. Ideally the locus of the input impedance should show up at the short–circuit point in the Smith chart. Instead the locus was shifted away from the ideal point. By changing the port extension, which is a measurement parameter of the network analyzer, I shifted the impedance into the short–circuit point. Then you also have to account for the additional length of the conductor that serves as the short between centerconductor and ground. This is done by increasing the port extension for a value that corresponds to half of this additional length[16]. With this procedure there still remains a certain phase error in the order of some degrees (the phase error without the last compensation is for this frequency range in the order of $10° - 15°$). The obtained value for the port extension was then used in every measurement. This procedure can also be understood as shifting the point of reference to the location where the feed line actually starts.

Beside the input impedance in the Smith chart, the return loss and the VSWR have also been measured. From the VSWR trace especially the bandwidth was extracted.

4.7.2 Radiation Pattern

The measurements of the antenna patterns have been performed in an anechoic chamber at the *Forschungszentrum Seibersdorf*[17].

The patch antenna operated as a receiving antenna and a horn was used as the transmitting antenna. The distance between the antennas was approximately $3m$. To check whether this distance is far enough to measure in the far–field region, we have to know where the far–field zone starts. An analytical border between the near–field

[15] The network analyzer system consists of a network analyzer HP 8510C, a S–parameter test set HP 8517A and a series synthesized sweeper HP 83651A.

[16] The issue here is to use the proper velocity factor, which accounts for the substrate parameters of the connector. This can only be found approximately by measuring the physical length of the connector and increasing the velocity factor at the network analyzer up to the value, where the analyzer shows the previous measured physical length. The velocity factor is the ratio of the effective versus free–space wavelength.

[17] Forschungszentrum Seibersdorf, Industrielle Meßtechnik und Informationsverarbeitung, A — 2244 Seibersdorf

zone and the far–field zone (for antennas with dimensions larger than the free–space wavelength λ_0) is given by the Rayleigh distance [29] r_{ff}

$$r_{ff} = \frac{2D^2}{\lambda_0}, \tag{4.6}$$

where D is the maximum dimension of the antenna. The full far–field conditions are summarized as follows:

$$r > r_{ff}, \quad r \gg D, \quad r \gg \lambda_0. \tag{4.7}$$

For the single element the maximum dimension is approximately $\lambda_0/2$. The resulting Rayleigh distance is then $r_{ff} \approx \lambda_0/2$. Therefore the far–field region can be found in a distance $r \gg \lambda_0$. Note that to measure deep nulls in the antenna pattern a sensor distance of at least $r = (5-10)r_{ff}$ is required. This is given for a distance of 3m, since $10\lambda_0 = 1.2m$.

4.8 Measurement Results and Comparison with Simulations

This section presents the achieved results for the single element antenna and compares them with the simulations.

4.8.1 Input Impedance and Bandwidth

The results for the input impedance plotted in the Smith chart are presented in Figure 4.9. The figure includes the measurement (solid line) and the simulation result (dashed line). You can find an excellent match between the two loci. Additionally the input impedance at the frequency of 2.44GHz has been emphasized.

From this point and from the fact that the measured locus is shorter than the predicted one a slight difference in the frequency behaviour can be observed. Actually, the measured trace showed a higher resonant frequency than the simulation. The compressed locus of the measurement (The locus has a shorter length although the frequency range is for both — measurements and simulation — the same.) means that the implemented antenna is stronger frequency dependent than the simulated antenna. This will — as you will soon see — cause a larger bandwidth.

The return loss over the frequency is shown in Figure 4.10. Again, the measured and simulated traces are plotted. The measured bandwidth is 180MHz, while 153MHz has been obtained from simulations. Most important is the fact that the requirements for the bandwidth are more than fulfilled. Another important conclusion from the last two figures is that the simulation tool gives accurate results to predict the performance of this structure.

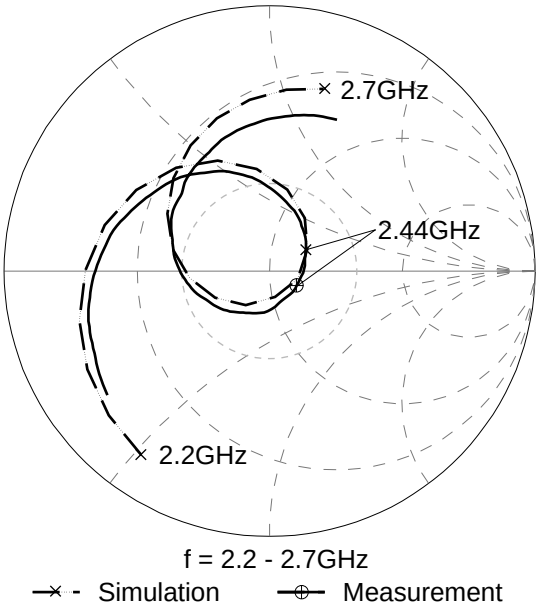

Figure 4.9: Comparison between measured and simulated input impedance of the single element antenna for a frequency range from $2.2 - 2.7GHz$.

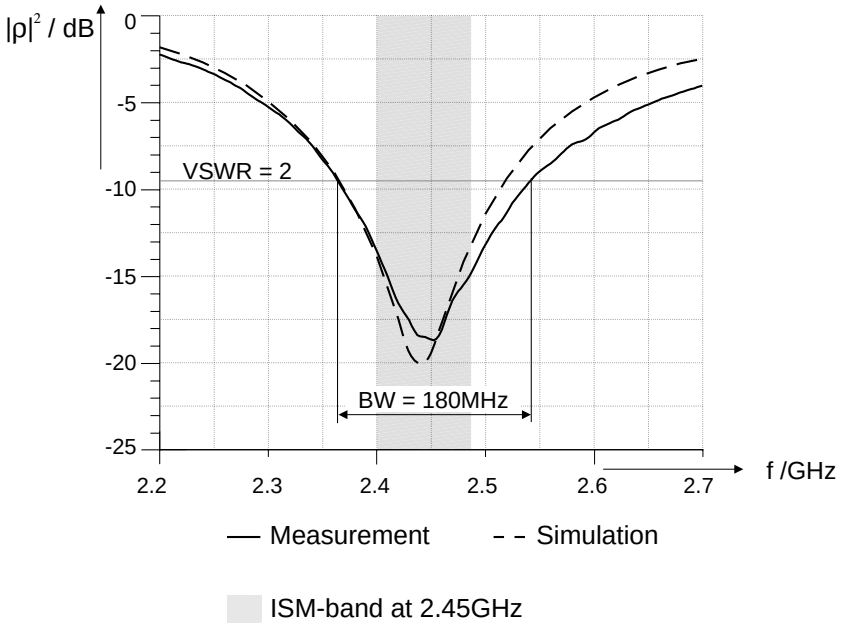

Figure 4.10: Comparison between measured and calculated return loss of the single element antenna for a frequency range from $2.2 - 2.7GHz$.

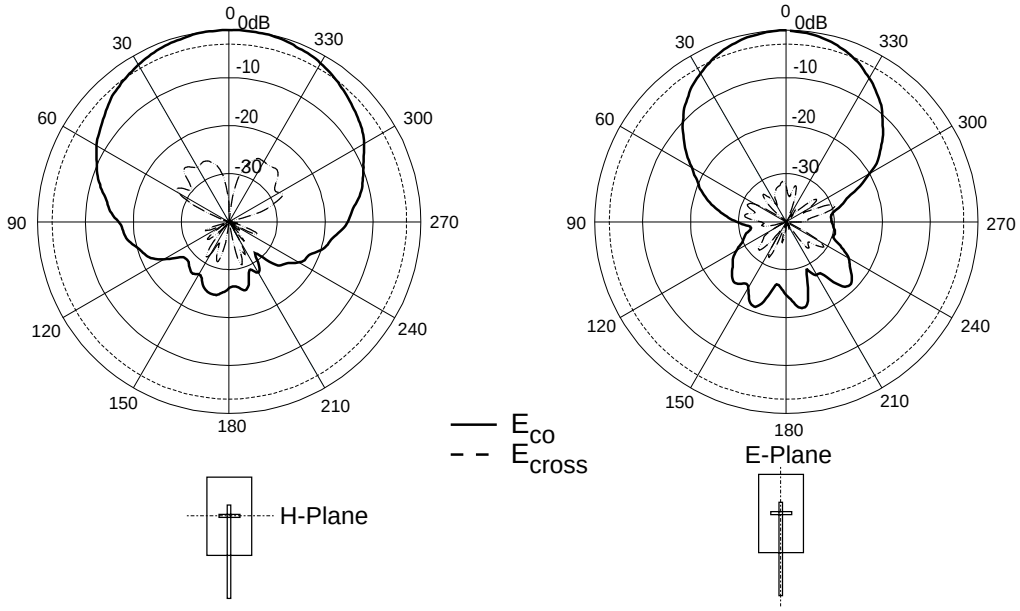

Figure 4.11: Measured vertical radiation pattern of the single element antenna at a frequency of 2.45GHz.

4.8.2 Radiation Pattern

The results for the vertical radiation pattern in H– and E–plane are shown in Figure 4.11. Both diagrams include the measurement results for the co– and cross–polarization component.

In comparison to the E–plane a wider mainlobe can be observed in the H–plane pattern. The front–to–back ratio for the H–plane of $F/B_H = 19.1dB$ was a little bit lower than the one in the E–plane ($F/B_E = 19.6dB$). The polarization purity in the E–plane ($XPP_E = 29.3dB$) was higher than in the H–plane ($XPP_H = 25.3dB$).

Figure 4.12 compares the simulated and the measured H–plane pattern for the case *without* (left diagram) and *with* (right diagram) the reflector. The measurement without the reflector has been performed to find out the improvement of the front–to–back ratio due to the reflector. And also to compare the radiation pattern with the one obtained by the simulation tool MultiStrip. In Table 4.5 you can find a summary of this comparison.

The gain in front–to–back ratio was measured to be 3dB. You maybe think that this is a rather small value, but bear in mind that I have defined the front–to–back ratio over the in both hemispheres radiated powers (see Chapter 1). If you compare the values of the normalized power pattern at 180° from the measurement with and without the reflector, you will find an improvement of approximately $8dB$ due to the reflector.

The fit between simulation result of MultiStrip (case without the reflector) and the

Table 4.5: Comparison of F/B–values simulated and measured in the H–plane.

	Without Reflector	*With Reflector*
Simulation	18.8dB	∞
Measurement	15.9dB	19.1dB

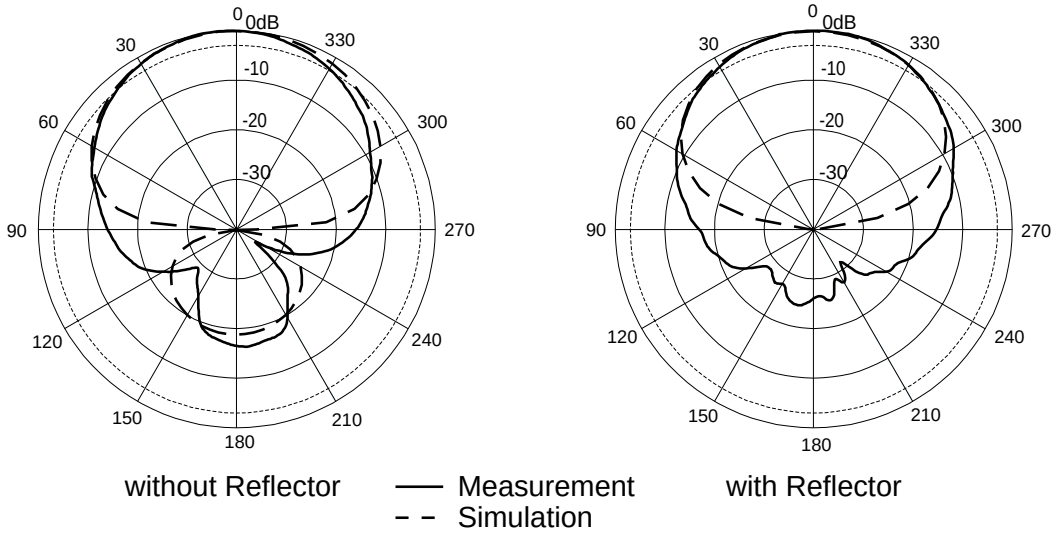

Figure 4.12: Comparison between measured and simulated normalized power pattern of the single element antenna for the H–plane at a frequency of 2.45GHz.

measurement result seems very well for the mainlobe. Just in direction of the ground plane ($\theta = 90°$ and $\theta = 270°$) there is a larger deviation between the two curves. This can be easily explained, when you remember that MultiStrip assumes an infinitely large ground plane. Of course the simulation result will then predict no radiation in that direction. In reality the ground plane is always of finite size and therefore a certain amount of radiation in direction of the horizontal plane is observed.

For the situation with the reflector the prediction of the back radiation failed. Again this is no wonder, since the reflector plane is assumed to have an infinite size. But we can also see that the simulated pattern meets the measured one very well in the mainlobe region.

A final pattern measurement has been performed in Seibersdorf to determine the maximum gain of the antenna: The horizontal pattern of a half–wavelength dipole was measured.

Figure 4.13 shows the result of this measurement and also includes the antenna pattern of the patch antenna in the H–plane. To determine the gain of the patch antenna I have to calculate the maximum gain over the dipole G_{dipole}. Since the

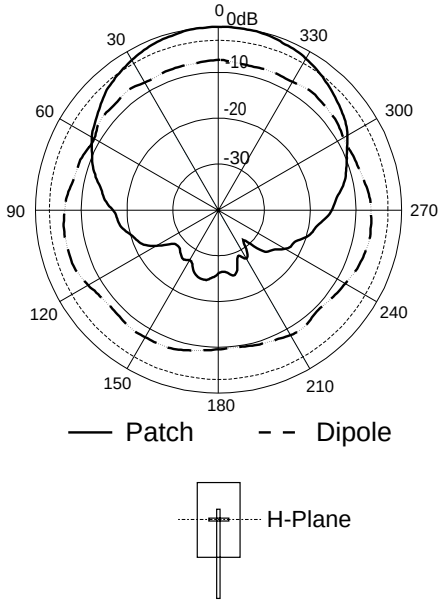

Figure 4.13: Measured radiation pattern of the single element patch antenna versus a dipole at a frequency of 2.45GHz.

directivity of a dipole (in comparison to the isotropic radiator) is well known (2.15dB [29]) from theory, the maximum gain G of the antenna can then easily be computed — by assuming that the dipole has no losses and therefore an antenna efficiency of 100% — from

$$G = G_{dipole} + 2.15dB. \tag{4.8}$$

But, the problem is to calculate G_{dipole} from the measured data. G_{dipole} is computed by subtracting (in logarithmic scale) the radiation intensity of the dipole from the maximum value of the measured radiation intensity of the patch antenna — $G_{dipole} = U_{max,patch} - U_{dipole}$. Unfortunately the dipole shows an antenna pattern that is not omnidirectional as known from theory. Actually the deviation from the omnidirectional pattern is in this case in the order of $\pm 2dB$.

Therefore the gain can only be predicted with an error of $\pm 2dB$! And this neglects any other measurement errors, for example due to a mismatched polarization[18]. Nevertheless I have computed such 'maximum gains' and used different values as the reference U_{dipole} — the maximum, the mean and the minimum value.

Table 4.6 lists the results: It shows that the minimum gain, calculated from this measurement, is $8.1dBi$. Compared to a simulated value for the case without the reflector of $8.4dBi$ the order of the measured maximum gain seems appropriate. Most

[18] Actually I measured in the E–plane pattern a maximum radiation intensity that was 0.6dB larger than that in the H–plane. Of course they should be the same!

Table 4.6: Calculated values for the maximum gain at 2.45GHz from measurement data in the H–plane.

Referred to	G
U_{max}	8.1dBi
U_{mean}	9.8dBi
U_{min}	11.9dBi

important is the fact that the antenna has a gain — and this is uncontested[19]! Table 4.7 finally summarizes the measurement results for the single element antenna (including the reflector) and compares them with the simulation results.

[19] From the radiation pattern we can see the patch antenna received more power in a specific angular section than the dipole. The determination of an accurate value is just the problem.

Table 4.7: Summary of the performance of the single patch antenna.

Parameter		*Simulated*	*Measured*
Bandwidth		$153MHz$	$180MHz$
Directivity D		8.7dBi	—
Efficiency η		91%	—
Maximum Gain G		8.3dBi	$8.1 - 11.9dBi$
Front–to–Back Ratio F/B	H–plane	$18.8dB$[a]	$19.06dBi$
Half–power Beamwidth		$86°$[a]	$74°$
-10dB Beamwidth		$140°$[a]	$135°$
Polarization Purity		∞	$25.3dB$
Front–to–Back Ratio F/B	E–plane	$16.6dB$[a]	$19.6dB$
Half–power Beamwidth		$68°$[a]	$47°$
-10dB Beamwidth		$122°$[a]	$89°$
Polarization Purity		∞	29.3dB

[a] The simulation does not include the reflector.

Chapter 5

Antenna Array

After realizing an optimized single element antenna the last step was the design and implementation of the antenna array.

5.1 Array Design

As stated in the specification of this work (see Chapter 1) a linear array with nine elements had to be implemented. We decided to implement a H–plane array, since with this configuration no space problems due to the single feed lines arose. Figure 5.1 shows the configuration of the array from a top view. To identify each single antenna the elements have been numbered.

A critical design parameter in this array is the rather small element spacing of a half free–space wavelength. Usual arrays use a patch width in the order of $0.4 - 0.5\lambda_0$. Then the remaining distance between the non–radiating edges would only be $0.1\lambda_0$ or less (see Figure 5.2 (a)). This small distance would cause extremely high mutual coupling. Therefore the patches are made narrower and I actually used a patch width in the order of $W_p \approx 0.2\lambda_0$. Then a distance of approximately $0.3\lambda_0$ remains between the non–radiating edges (see Figure 5.2 (b)).

Unfortunately the bandwidth of a microstrip patch antenna decreases with decreasing patch width (see Section 2.2.6 at page 18). This degradation in bandwidth

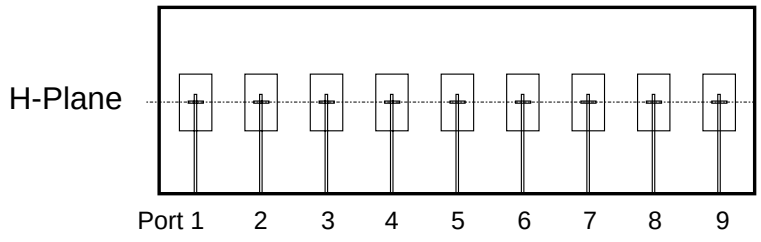

Figure 5.1: Top view of the antenna array.

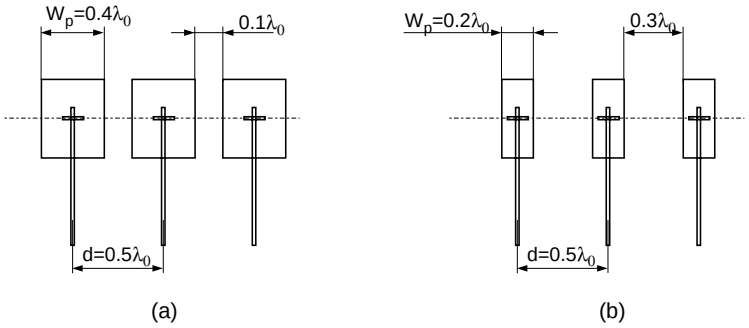

Figure 5.2: Array configurations for different patch widths.

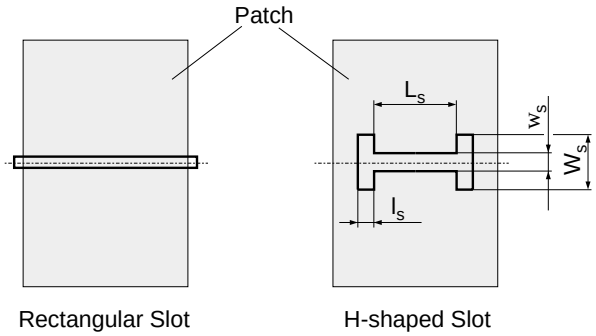

Figure 5.3: Slot configurations with different slot shapes.

performance was compensated by using a thicker patch substrate. Due to this increase of the distance between the patch and the slot, the coupling factor was lowered. Therefore I had to increase the slot length to obtain a larger coupling factor. The slot length that was required to yield high enough coupling was finally *larger* than the width of the patch (see Figure 5.3).

This situation is of course undesired, since the mutual coupling is then increased again and the narrow patches make no sense any more. Therefore another slot geometry was used — a H–shaped slot (see Figure 5.3). With this slot geometry the polarization purity is a little bit lowered due to the additional parts of the slot that are perpendicular to the conventional slot. Another performance parameter that is degraded is the front–to–back ratio. This comes from the larger slot area in comparison to the single element configuration.

The remaining part of the design (matching and tuning) was then similarly carried out as the single element design. The final geometry for a single element of the array is listed in Table 5.1.

Table 5.1: Geometry of the antenna array.

Antenna Part	*Parameter*	*Value*
Cover Substrate	Relative Permittivity ε_{r_c}	3.38
	Height H_c	0.2mm
	Losses $\tan\delta_c$	$2{\cdot}10^{-3}$
Patch	Length L_p	45.8mm
	Width W_p	23.0mm
Patch Substrate	Relative Permittivity ε_{r_p}	1.09
	Height H_p	8.1mm
	Losses $\tan\delta_p$	$2{\cdot}10^{-4}$
Slot	Length L_s	16.9mm
	Length l_s	1.54mm
	Width W_s	5.1mm
	Width w_s	1.7mm
Patch Substrate	Relative Permittivity ε_{r_f}	3.38
	Height H_f	0.81mm
	Losses $\tan\delta_f$	$2{\cdot}10^{-3}$
Feed Line	Length L_f	77.9mm
	Width W_f	1.88mm
	Stub Length L_{stub}	8.4mm

5.2 Simulation Results

The most important simulation results are presented in this section. As already mentioned in Chapter 3 the array has also been calculated with another simulation tool — with Ensemble (see Chapter 3).

Table 5.2 will summarize the most important simulation results that have been obtained from both programs. Note that MultiStrip results are only for a single element of the array (only the mutual coupling at resonant frequency between two neighbouring elements in a three element array has been computed). Both programs cannot account for the finite reflector. From the simulation results for the whole array (Ensemble) I only took the results for the center element (element 5) and one for the most outward elements (element 1).

After having got an overview of the performance of the array, I will discuss the results in more details.

5.2.1 Input Impedance and Bandwidth

In Figure 5.4 you can find the simulated input impedance presented in the Smith chart. The black plotted locus shows the result from MultiStrip, while the grey loci have been

Table 5.2: Performance of the simulated antenna array.

	MultiStrip	*Ensemble*	
Parameter		Element 1	Element 5
Bandwidth	$201MHz$	$167MHz$	$155MHz$
Directivity D	$8.6dBi$	—	—
Efficiency η	87%	—	—
Maximum Gain G	$8.0dBi$	$8.65dBi$	$7.99dBi$
Front–to–Back Ratio F/B H–plane	$19.0dB$	$19.8dB$	$19.4dB$
Polarization Purity	∞	$46.6dB$	$44.9dB$
Maximum Mutual Coupling	$-15.9dB$	$-15.5dB$	$-14.4dB$

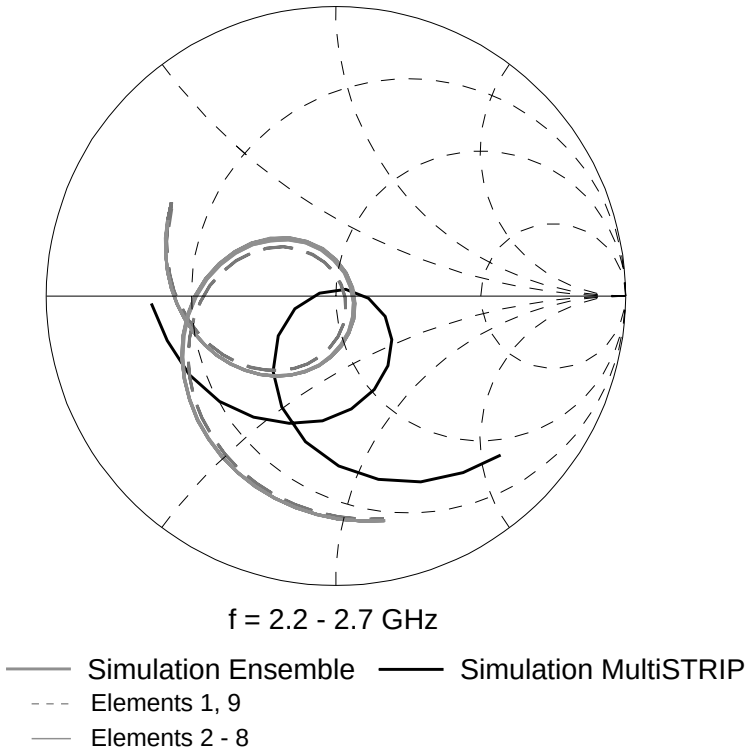

Figure 5.4: Simulated input impedance for the frequency range from $2.2 - 2.7GHz$.

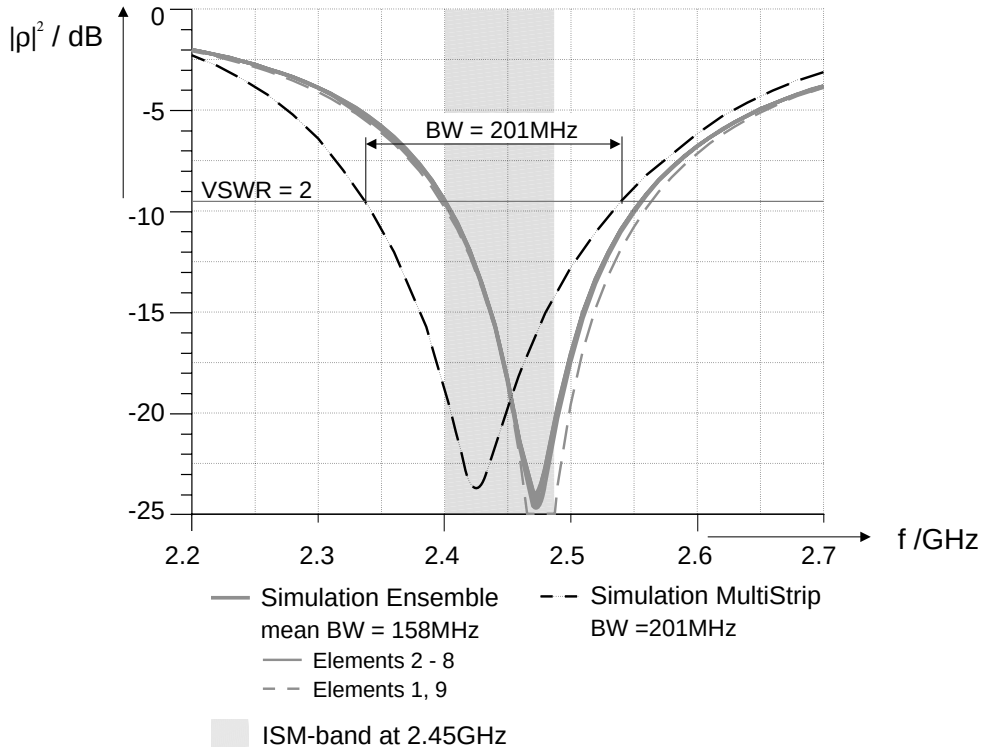

Figure 5.5: Simulated return loss for a frequency range from $2.2 - 2.7GHz$.

calculated by Ensemble. First of all you can observe a rather large phase deviation of the two simulated results. This is mainly due to the fact that I could not use the exact feed line length for the simulation in MultiStrip, because otherwise some other geometry parameters would have not been right (see also Chapter 3). The chart also shows two different traces from Ensemble. The solid grey line shows the results of all inner elements (elements $2 - 8$) — which means all elements except the two most outward ones. The loci for these seven elements lie close to each other and therefore you can only see one thicker plot. The dashed line represents the results for the two most outward elements (elements 1 and 9). This behaviour can be easy explained by reminding the array geometry. The two most outward elements have one nearest neighbour, while all other elements have to face two nearest neighbours and therefore they are more influenced due to mutual coupling.

Figure 5.5 shows the result for the return loss over the frequency. Here we also find a strong difference in the frequency behaviour between the predictions from Ensemble and MultiStrip. Since I tuned the patch substrate parameter in the MultiStrip simulations, the prediction of the resonant frequency is very accurate (see Figure 5.11 on page 66). For the simulations with Ensemble we used the nominal values for the patch substrate parameters and included the thin adhesive layers. As you can see, Ensemble predicts a minimum for the return loss that is approximately $40MHz$ larger than that

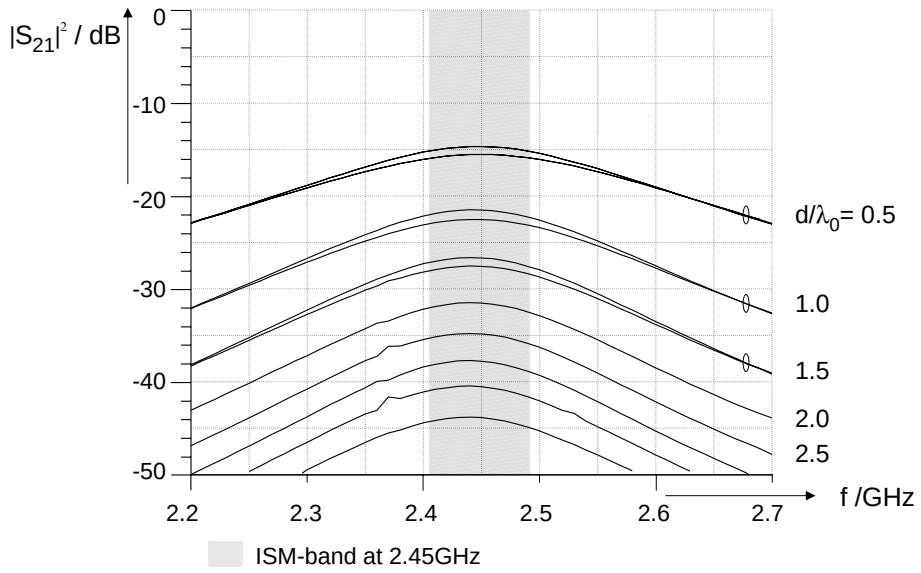

Figure 5.6: Simulated (Ensemble) mutual coupling for a frequency range from $2.2 - 2.7GHz$.

calculated by MultiStrip. One possible reason for this deviation (which also occurs in comparison to the measurement results) is that the patch substrate permittivity is in reality somewhat larger. This can also fit with the simulation result I got from MultiStrip, since there I increased the permittivity until I have been able to predict the resonant frequency accurately. And this procedure does not care about what the purpose for the lower resonant frequency is — the adhesive layers or the wrong patch substrate permittivity.

Nevertheless it is interesting to see that MultiStrip predicts a much larger bandwidth than Ensemble does. This comes from the fact that the MultiStrip results do not include any mutual coupling. So the conclusion from this is that the mutual coupling lowers the bandwidth considerably.

5.2.2 Mutual Coupling

From Ensemble I also got predictions for the mutual coupling over the frequency for the whole array, while with MultiStrip I only calculated the value for the center frequency.

Before I continue, I want to note that the mutual coupling is originally defined by the impedance (or Z–) matrix. Since I cannot measure the Z–parameters, I quantify the mutual coupling with the transmission coefficients — or the S–parameters. These can be easily measured with a network analyzer.

Figure 5.6 shows the transmission coefficients for a selected number of pairs of single elements over the frequency. The parameter in this figure is the distance d between the single elements, where curves for all distances $d/\lambda_0 = 0.5 \ldots 4$ are drawn. The two

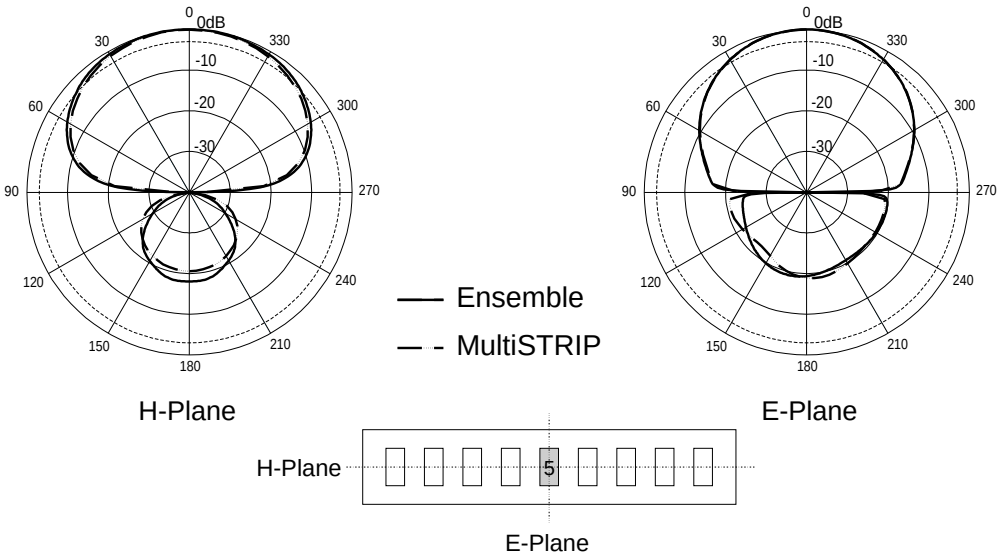

Figure 5.7: Simulated normalized power pattern for the center element at a frequency of $2.45GHz$.

topmost traces (that are labeled with $d/\lambda_0 = 0.5$) show the transmission coefficient (in the following named S_{ij}) for the element pairs $i = 1, j = 2$ (lower curve) and $i = 4, j = 5$ (upper curve). Similar is the situation for the curve where d/λ_0 is unity, where S_{13} and S_{46} are plotted. The bottommost plot shows S_{19}.

From these simulations we can see that the largest values for the mutual coupling can be found near the resonant frequency. The maximum mutual coupling occurs for S_{45} with $-14.4dB$.

5.2.3 Radiation Pattern

The simulated vertical normalized power pattern for the center element in E– and H–plane at $2.45GHz$ is presented in Figure 5.7. Note that in these calculations the influence of the reflector is not included, and that the MultiStrip result is for only one single element, while Ensemble calculated for every element an antenna pattern. The comparison between the simulation results of the two programs shows only slight deviations in the back radiation, while in the upper hemisphere an excellent conformity is given. I also want to note that both programs predicted the same gain of $G = 8dBi$, although MultiStrip does not account for mutual coupling and Ensemble does. Note that Ensemble predicts a little bit larger maximum gain for the most outward elements ($G = 8.65dBi$).

To estimate the largest possible directivity of the nine element array an equiphased array had been simulated and the result is presented in Figure 5.8. This figure includes the normalized power pattern for both the H– and E–plane. Due to the H–plane array

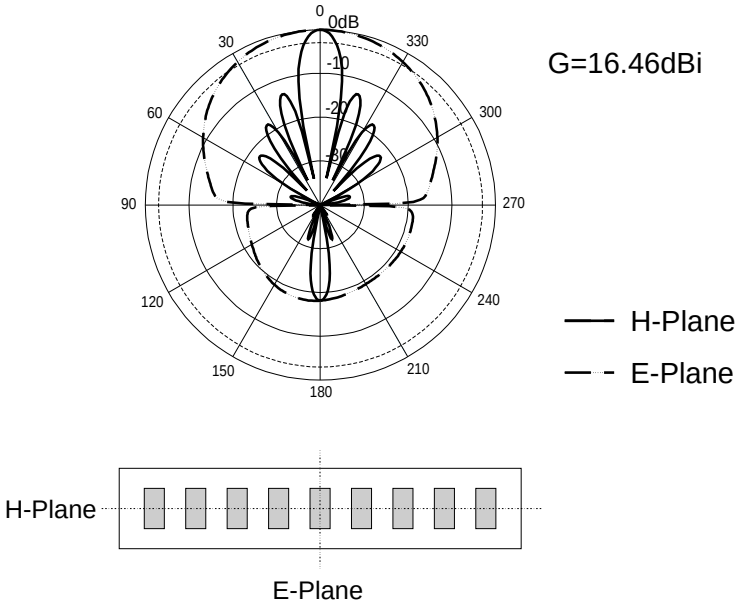

Figure 5.8: Simulated normalized power pattern for an equiphased nine element array (Ensemble).

configuration, the E–plane pattern is the same as for the single element. The calculated maximum gain for the nine element array is $G = 16.46dBi$. The improvement in gain due to the array lies between $G_{array} = (7.8 - 8.5)dBi$[1]. From array theory [15] the directivity of a N element equiphased array with element spacing of $d = m\lambda_0/2$ $(m = 1, 2, 3 \ldots)$ that consists of isotropic radiators is calculated to

$$G_{N-array} = 10 \log_{10} N. \tag{5.1}$$

For a nine element array this results in $G_{9-array} = 9.54dBi$. The reason for the lower simulated array gain than that given by theory is the mutual coupling, which is not included in the theoretical approach.

5.3 Implementation

The major part of the implementation of the antenna array was similar to the single element fabrication. Here I will only discuss the new tasks that had to be done and the difficulties that occurred.

[1]The improvement in gain is the difference between the array gain and the single element gain.

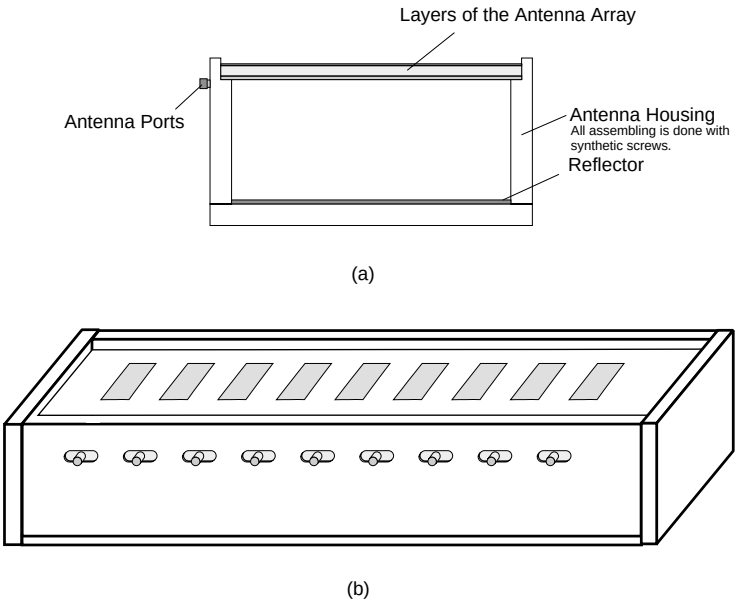

Figure 5.9: Housing of the antenna array. (a) Cross–section. (b) Perspective view.

Printed Structures

The whole array was too large to be manufactured at once; therefore I splitted it in three groups each containing three single elements.

Antenna Housing

Since I want to protect the antenna against environmental effects, it must be built in a proper housing. Of course I could not take any metal for the housing, therefore we used — transparent — sheets of acrylic glass. With a clever design, the spacer that holds the reflector could be omitted. The synthetic screws, required to align the different layers, have also been omitted. The alignment of the layers was accomplished with small drills in the different layers and with thin metal pins that have been removed after the substrates have been sticked together. Figure 5.9 shows a simplified schematic of the antenna housing.

5.4 Performing the Measurements

5.4.1 Input Impedance, Bandwidth and Mutual Coupling

The measurements of the input impedance and the bandwidth have been carried out similarily as the single element measurements (see Section 4.7). Nevertheless an additional condition has to be fulfilled due to the 9–input ports: All in the current

measurement unused ports have to be loaded with a terminator (50Ω resistor). This condition comes from the definition of the S–parameters. If the unused elements are not terminated, a strong deviation in the measurement results has been observed. In the final array implementation the difference occurred especially near the lower band limit ($2.4GHz$) and caused a decreased bandwidth due to an increased mutual coupling. So again, to get reliable and accurate results all other input ports have to be terminated!

5.4.2 Radiation Pattern

The measurements of the array antenna pattern have been performed in an anechoic chamber at the *Institut für Hochfrequenztechnik of Prof. F. Landstorfer at the Universität Stuttgart*[2].

The anechoic chamber in Stuttgart has a size of $14.4m \times 6m \times 6m$, which made a distance of $7m$ between the receiver antenna (patch array) and the transmitter antenna (horn) possible.

From Equation 4.6 the Rayleigh–distance of $r_{ff} = 4.2m$ is obtained, where a maximum array dimension of $D = 4.2\lambda_0$ is assumed. From this result we can see that the field was measured in the far–field region. However, I stated on page 48 that the field should be measured in a distance of $(5 - 10)r_{ff}$ from the antenna[3], which is not given for $r = 7m$. In the next section you will see that the emphasize lies on the measurement of the single element antenna pattern. For the single element measurements the unused antenna elements are only parasitic radiators with less contribution to the antenna pattern. Therefore a maximum dimension of $D = 4.2\lambda_0$ is a rather high value. Finally I want to note that in the measured antenna pattern deep nulls have been observed.

For the pattern measurements the same condition as for the S–parameter measurements has to be fulfilled: All unused antenna elements during a measurement cycle have to be terminated!

5.5 Measurement Results and Comparison with Simulations

5.5.1 Input Impedance and Bandwidth

Figure 5.10 shows the measured input impedance for the nine input ports. The shaded area in the Smith chart represents the region, where all nine loci of the measured input impedance are within, while the solid dark grey line denotes the result for the center element. The figure additionally includes the simulation result for the center element (Ensemble), plotted with a black dashed line.

[2]Institut für Hochfrequenztechnik, Universität Stuttgart, BRD – 70550 Stuttgart, Pfaffenwaldring 47.

[3]This is required to be able to measure deep nulls in the antenna pattern.

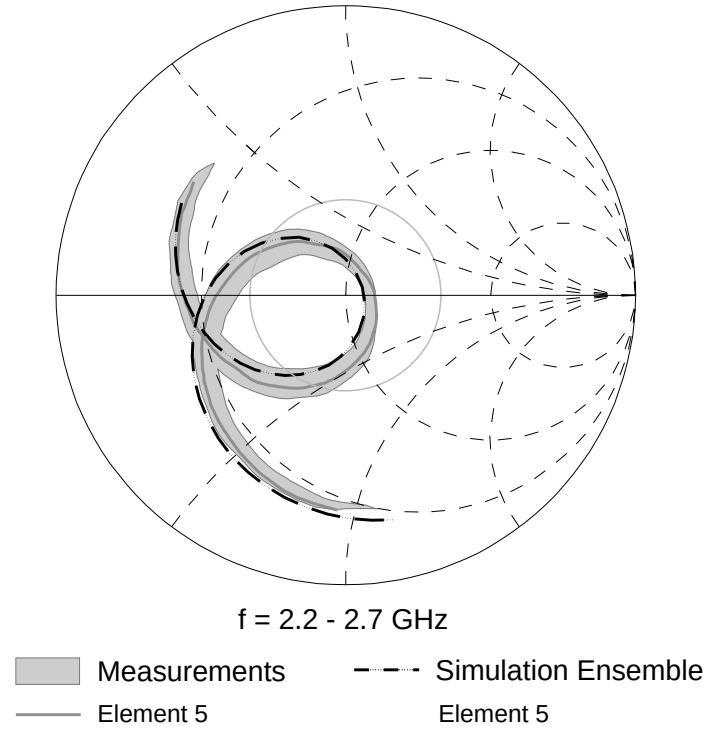

Figure 5.10: Comparison between measured and calculated input impedance for a frequency range from $2.2 - 2.7GHz$.

From the shaded area we can observe some phase differences between the single element loci that come from uncertainties in fabrication. Excellent agreement can be observed between the simulation result from Ensemble and measurement results.

Figure 5.11 shows the measurement result for the return loss. Again the shaded area represents the region, where all nine measured return loss traces of the single elements are included. The result for element 4 is emphasized (solid line), because it is the element with the minimum bandwidth ($BW = 158MHz$). The figure additionally includes a plot (dashed line) that shows the simulation result from MultiStrip.

The simulation predicted the resonant frequency accurately (because it was optimized to do this), but it calculates a higher bandwidth ($BW_{MultiStrip} = 201MHz$) compared to the measurement results. Table 5.3 lists the measured bandwidth of the single elements of the array. From this we can see that the bandwidth for all inner elements (2–9) is in the same order (approximately $162MHz$), while the elements 1 and 9 showed a larger bandwidth ($175MHz$). From this I conclude that the mutual coupling decreases the bandwidth, because the most outward elements have only one nearest neighbour and therefore face a less serious situation in terms of mutual coupling. Note that the simulation results of Ensemble also predicted such a behaviour.

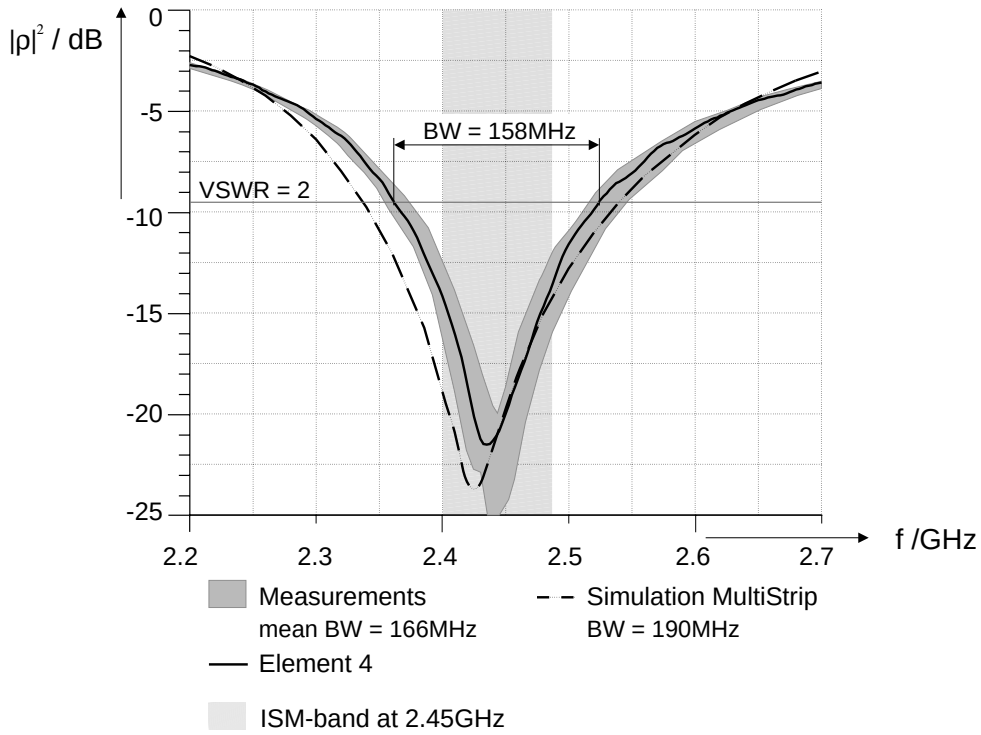

Figure 5.11: Comparison between measured and calculated return loss for a frequency range from $2.2 - 2.7GHz$.

Table 5.3: Measured bandwidth of the single elements of the antenna array.

Antenna Element	*Lower band limit*	*Upper band limit*	*Bandwidth*
1	$2.358GHz$	$2.532GHz$	174MHz
2	$2.372GHz$	$2.507GHz$	165MHz
3	$2.363GHz$	$2.527GHz$	164MHz
4	$2.357GHz$	$2.515GHz$	158MHz
5	$2.363GHz$	$2.525GHz$	162MHz
6	$2.359GHz$	$2.525GHz$	166MHz
7	$2.368GHz$	$2.533GHz$	165MHz
8	$2.370GHz$	$2.538GHz$	168MHz
9	$2.363GHz$	$2.538GHz$	175MHz

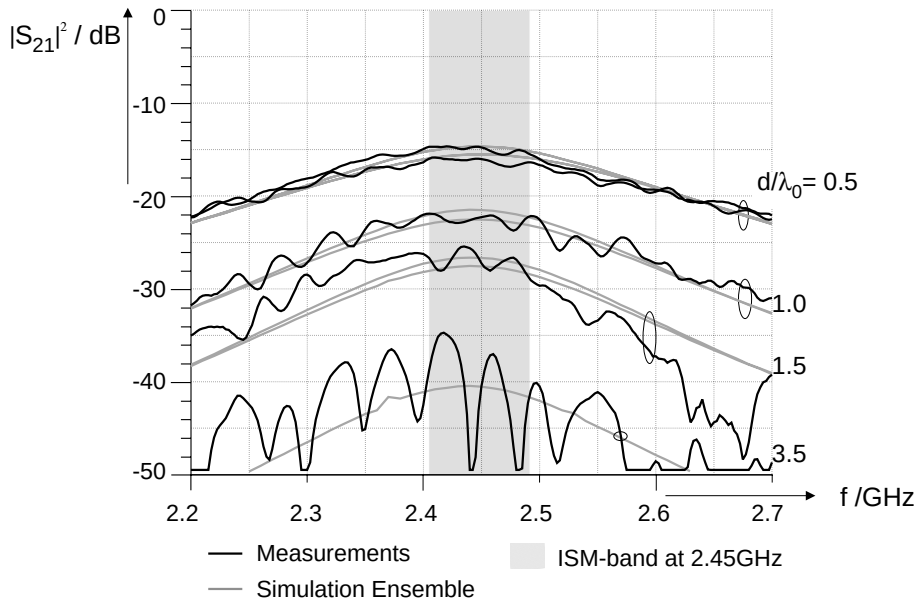

Figure 5.12: Comparison of measured and simulated (Ensemble) mutual coupling.

The most important conclusion drawn from this figure is that the requirement for the bandwidth ($BW > 120MHz$) is more than fulfilled, since the minimum bandwidth is $BW_{min} = 158MHz$. Therefore enough margin in bandwidth remains on both sides of the ISM–band limits.

5.5.2 Mutual Coupling

Figure 5.12 presents some of the measured transmission coefficients over the frequency with the normalized distance d/λ_0 as parameter. The figure compares the measurement results (black lines) with the from Ensemble calculated traces (gray lines). For $d/\lambda_0 = 0.5$ the measurements show the best agreement with the simulation result (S_{54} — topmost curve and S_{12} — below S_{54}). The traces showed a ripple that gets larger with increasing distance. Especially in the traces for $d/\lambda_0 = 3.5$ you can observe a ripple that is already in the order of $15dB$. But note that the order of the predicted mutual coupling agrees very well with the measured traces. The maximum value of the measured mutual coupling was $-14.5dB$ and occured for S_{45}.

In Figure 5.13 the maximum values for the mutual coupling are plotted over the distance. Here the maximum values of the mutual coupling within the ISM–band have been measured for all possible combinations of single elements. Values for the same distance — for example for $d/\lambda_0 = 0.5$ the measurement results of S_{12}, S_{23},..., S_{89} — are averaged and the mean value is drawn with the black solid line. It is self–evident that for larger distances fewer measurements could have been performed and finally for $d/\lambda_0 = 4$ only one value S_{19} is available. The error bars included in this figure represent the maximum deviation of the measurement results from the mean value.

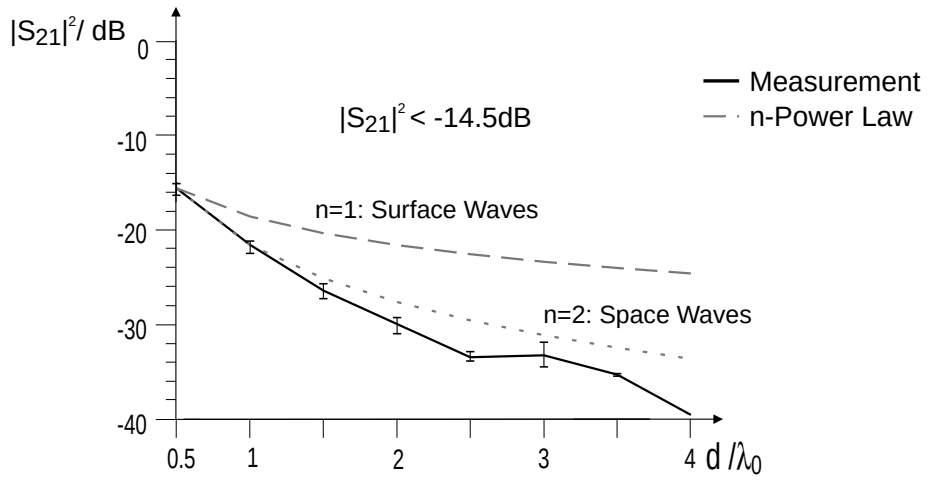

Figure 5.13: Measured maximum mutual coupling within the ISM–band over the element spacing.

Additionally the figure includes two n–power law curves $P(n)$. These plots show the decrease in power with an exponent n over the distance:

$$P(n) = -14.5dB - 10\log_{10}(d^n) = -14.5dB - n10\log_{10} d \tag{5.2}$$

The traces are referred to the maximum value of the mutual coupling of $-14.5dB$. The curve for $n = 1$ shows the decrease of power of a surface wave (compare Section 2.2.4), while for $n = 2$ the power decrease of a space wave is represented. From these figures we can see that the behaviour of the maximum measured mutual coupling lies near the case of the space wave and not near the surface wave configuration! This means that there are no significant excitations of surface waves that could increase the mutual coupling and also degrade the performance of the antenna in terms of antenna efficiency.

5.5.3 Radiation Pattern

This section presents a selection of the most important antenna pattern measurements.

Figure 5.14 shows the measured vertical radiation pattern of the center element at $2.45GHz$ for the H– and E–plane. The solid line represents the measured co–polarization component, while the dashed line shows the cross–polarization component. Similar to the results for the single element antenna (see Section 4.8) the H–plane pattern showed a wider main lobe than the E–plane. The polarization purity was in the H–plane higher ($XPP_H = 24dB$) than in the E–plane ($XPP_E = 20.3dB$). The polarization purity is worse compared to the results for the single element, and this comes mainly from the fact that a H–shaped slot is used in the array.

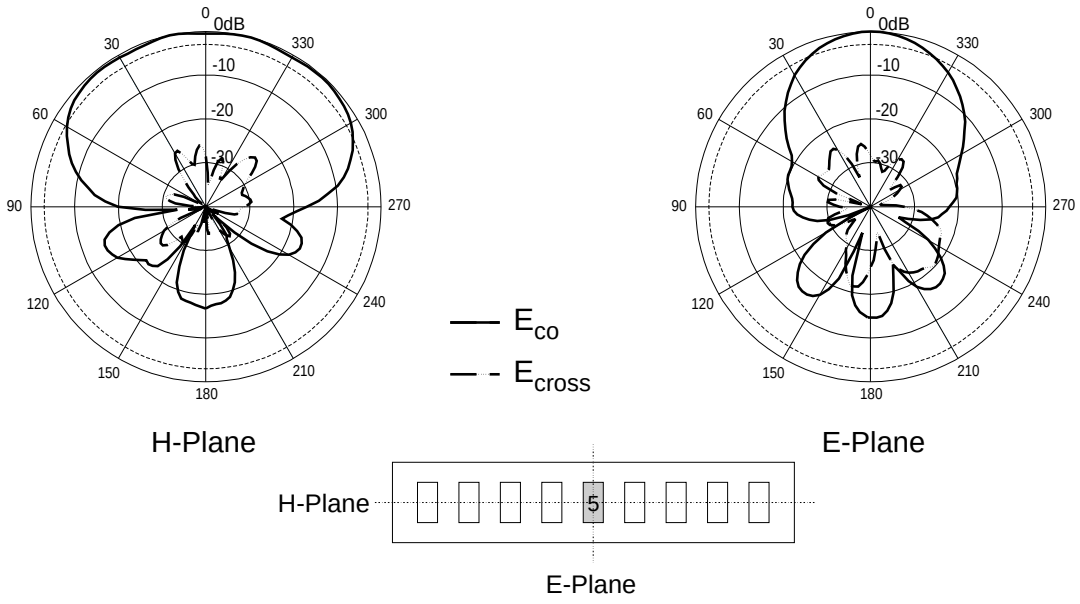

Figure 5.14: Measured vertical radiation pattern of the center element at a frequency of $2.45GHz$.

A front–to–back ratio in the H–plane of $F/B_H = 17.8dB$ was measured, while in the E–plane a value of $F/B_E = 17.4dB$ has been observed. The little bit lower value of the front–to–back ratio for the array in comparison to the single element result is caused by the larger slot area that is used in the array.

Figure 5.15 compares the H–plane pattern of some antenna elements. On the left–hand side we can see the pattern for the center element (referred to the maximum value of all plots within this figure), while on the right–hand side the antenna patterns for the two most outward elements are presented. Both diagrams also include the horizontal pattern of the half–wavelength dipole[4].

The pattern for the center element shows, as expected, an almost symmetrical behaviour, while the pattern for the elements 1 and 9 show a shift of the main lobe direction away from broadside. These two later patterns are almost symmetrical to each other corresponding to the z–axis ($\theta = 0$). This is a proof that the different element behaviour comes mainly from the mutual coupling and not from uncertainties in the fabrication of the antenna.

The measurement of the dipole was again performed to determine the gain of the antenna. When you compare the pattern for the dipole with the pattern that was measured in Seibersdorf (see Figure 4.13) you can find a smaller 'ripple' in the Stuttgart measurements ($2.13dB$). The reason for this is that in Stuttgart an antenna rack was used that influences the radiation pattern less. This result makes possible a more precise determination of the maximum gain of the antenna array. The following table

[4]Note that this dipole is the same as the one which was already measured in Seibersdorf.

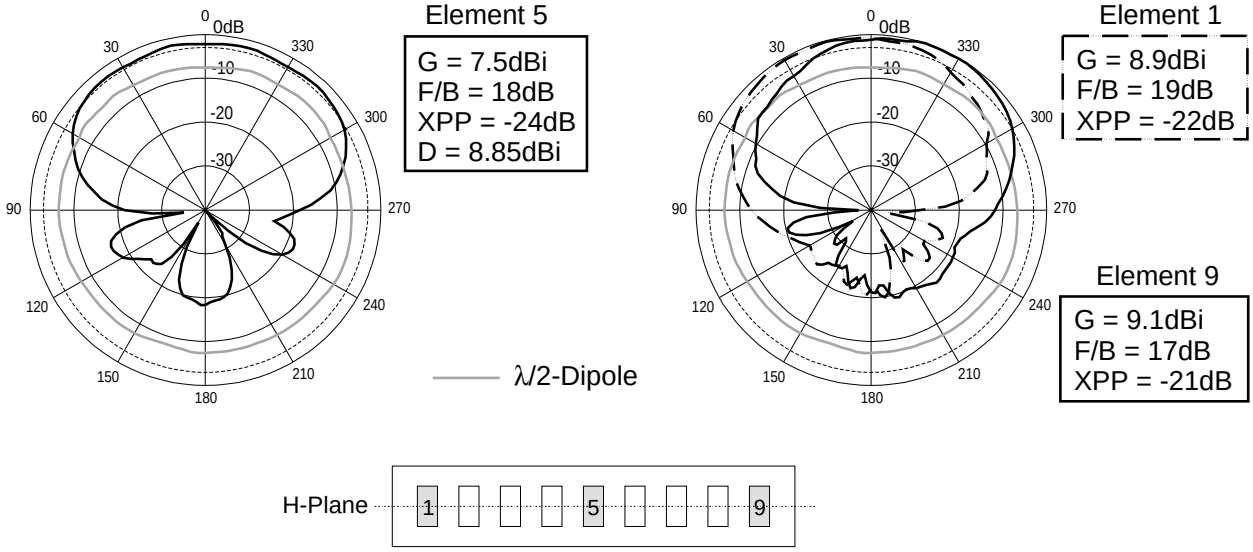

Figure 5.15: Measured vertical radiation pattern at a frequency of $2.45GHz$.

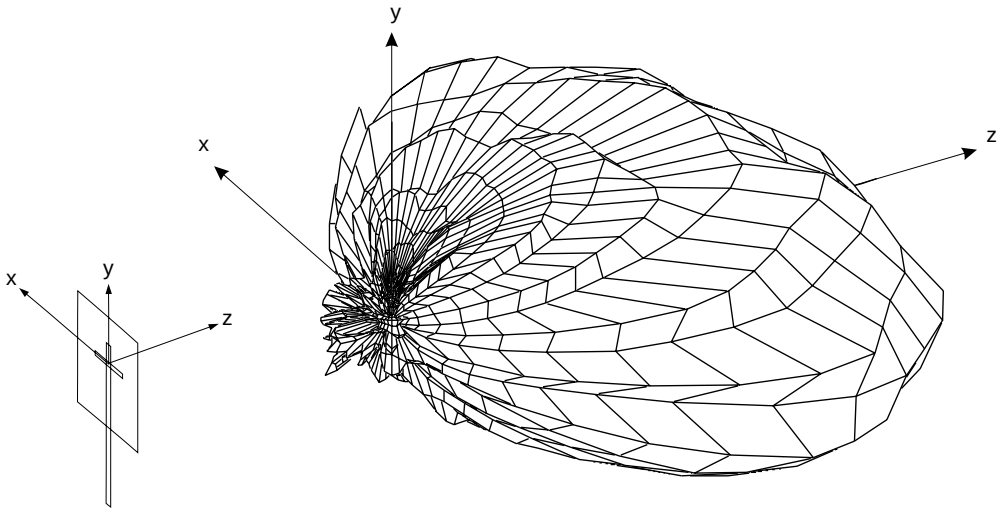

Figure 5.16: Measured radiation pattern over a whole sphere at a frequency of $2.45GHz$.

Table 5.4: Calculated values for the maximum gain G and the efficiency η at 2.45GHz from measurement data in the H–plane.

Element	*Referred to*	*G*	η
1	U_{max}	8.02dBi	—
5		6.57dBi	61.7%
9		8.22Bi	—
1	U_{mean}	8.93dBi	—
5		7.48dBi	72.4%
9		9.13dBi	—
1	U_{min}	10.15dBi	—
5		8.7dBi	96.7%
9		10.35dBi	—

lists the calculated maximum gains (with Equation 4.8) that are again referred to the minimum, mean and maximum radiation intensity.

First of all we find the smallest gain for the center element and a larger gain for the most outward elements — again this comes from the mutual coupling. Second, the gain for example for the center element is in the order of $7.5dBi$ with an error of approximately $\pm 1dB$ $(6.6 - 8.7dBi)$. The front–to–back ratio is for all elements in the order of $18dB$, while the polarization purity is about $22dB$.

For the center element the radiation pattern over a whole sphere has been measured and the result is presented in Figure 5.16. From this measurement the directivity for the center element has been computed by using Equation 4.5, where the maximum radiation intensity is divided by the mean value for the directivity. The result was a directivity of $D = 8.85dBi$. From the directivity and the maximum gain, the antenna efficiency can be calculated (see Equation 2.9). Depending on which value the gain is referred to, the in Table 5.4 listed efficiencies are computed.

An exact value for the efficiency cannot be computed, but you can see that the antenna efficiency is larger than 61%, which equals losses of only $2.1dB$ (worst case).

The result for the antenna efficiency and the result for the decrease of the mutual coupling (see Figure 5.13) support the conclusion that the broad bandwidth of the antenna does not come from losses, but rather due to the proper selection of design parameters!

Figure 5.17 compares the simulated (Ensemble; without reflector) and the measured H– and E–plane pattern. For both diagrams the agreement in the upper hemisphere is rather good; note that Ensemble also predicts a small shift of the main lobe direction

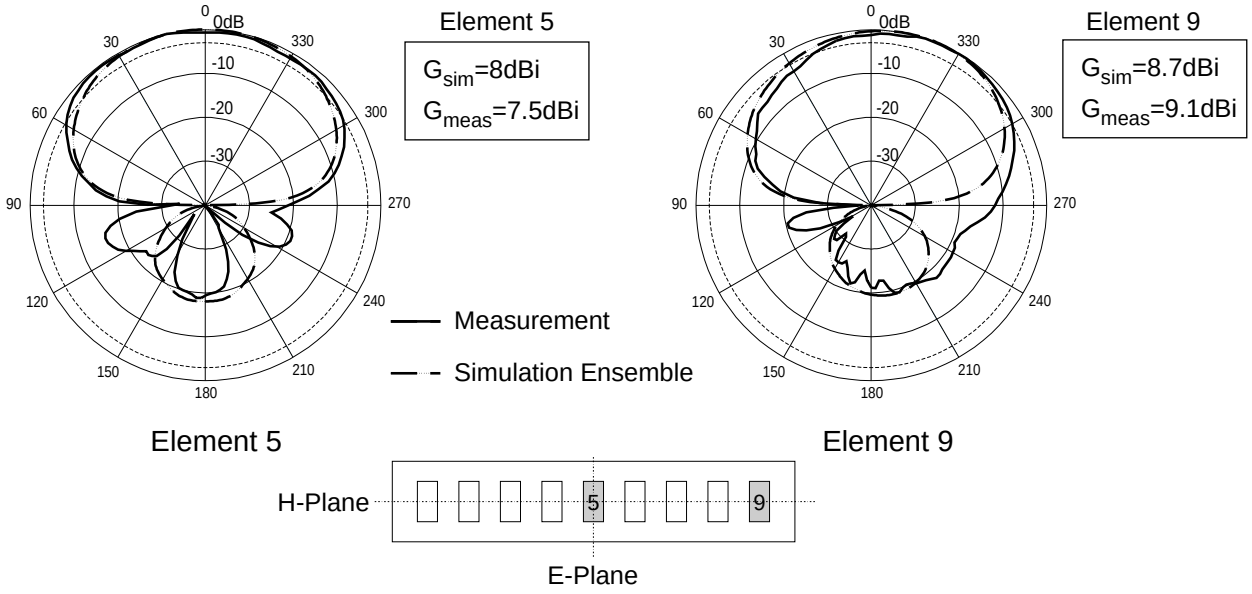

Figure 5.17: Comparison between measured and simulated (Ensemble) vertical radiation pattern in H–plane at a frequency of $2.45GHz$.

for the element 9. The simulation of course predicts a different antenna pattern in the lower hemisphere because it assumes no reflector.

Two final measurements of the antenna array have been carried out: The H–plane pattern of a 5–element and a 3–element equiphased array at 2.45GHz. The pattern (solid black lines) of the 5–element is presented in the left–hand diagram of Figure 5.18, while the right–hand diagram shows the result for the 3–element array. I also put into this figure simulated antenna patterns. Actually MultiStrip calculated the single element pattern. The array factor F_{array} is given by Equation 5.3. The overall pattern was then computed as the product of the single element field pattern and the array factor.

$$F_{array}(\theta) = \sum_{i=1}^{N} a_i \exp\left[j\pi\left(\sin\theta + b_i\frac{\pi}{180}\right)\right], \tag{5.3}$$

where N is the number of excited elements, a_n are the excitation amplitudes and b_n are the excitation phases in degree. The actual used beamforming network (consisting of power dividers and cables) was not constructed for the 2.45GHz range and showed therefore unequal phases and attenuations. These have been measured and the result is listed in Table 5.5.

From Figure 5.18 you can see that in both cases the agreement between simulation and measurements is very well. Although a real equiphased excitation does not exist, the directivity is only decreased insignificantly, while a remarkable difference in the sidelobe level behaviour can be observed.

The figure also includes the radiation pattern for the center element to get a feeling

Table 5.5: Measured amplitudes and phases of the beamforming network at 2.45GHz referred to the element with minimum attenuation.

Input Port	*Amplitude*	*Phase*
3	0.90	33.2°
4	0.98	0.95°
5	0.90	31.2°
6	0.91	29.1°
7	1	0°

for the gain of the array. The 5–element array shows of course a larger maximum gain ($12.8dBi$) than the 3–element ($10.5dBi$).

Table 5.6 summarizes the final results for the antenna array and compares them with the simulation. If more values have been simulated or measured, the table includes the worst case values for each performance parameter.

Table 5.6: Performance of the final antenna array.

Parameter	*Simulation*		Measurement
	MultiStrip	Ensemble	
Bandwidth	$201MHz$	$> 155MHz$	**> 158MHz**
Directivity D	$8.6dBi$	—	$8,85dBi$
Efficiency η	87%	—	$\approx 70\%$
Maximum Gain G	$8.0dBi$	$> 8.0dBi$	**> 7.5dBi**
Front–to–Back Ratio F/B H–plane	$19.0dB$	$> 19.4dB$	**> 17.1dB**
Polarization Purity	∞	$> 44dB$	$> 20.6dB$
Maximum Mutual Coupling	$-15.9dB$	$< -14.4dB$	$<$ **−14.5dB**

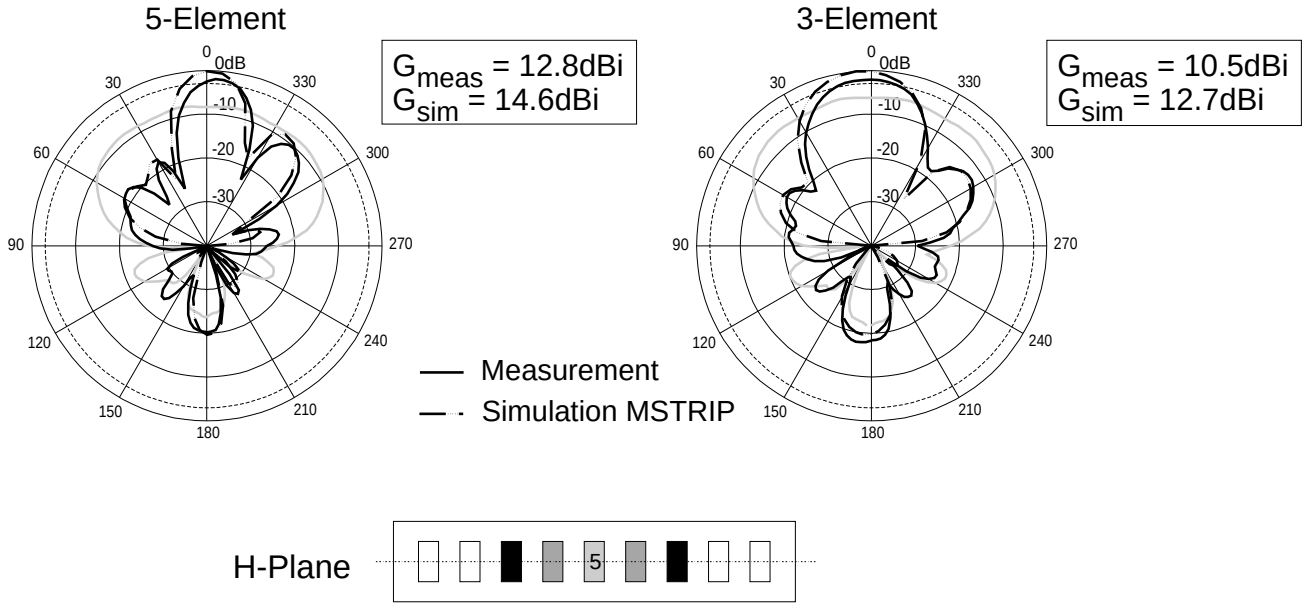

Figure 5.18: Measured vertical radiation pattern of equally excited arrays at a frequency of $2.45GHz$.

Appendix A

Fotos

Figure A.1: The antenna array and the author.

Foto 2

Figure A.2: The antenna array.

Foto 3

Figure A.3: The antenna array in operation.

Foto 3

Figure A.4: 3–dimensional pattern measurement in an anechoic chamber (Stuttgart).

Bibliography

[1] Inder J. Bahl and Prakash Bhartia. *Microstrip Antennas*. Artech House, Inc., Norwood (Mass.), 1980.

[2] Inder J. Bahl and Prakash Bhartia. *Microwave Solid State Curcuit Design*. John Wiley & Sons, Inc., New York, 1988.

[3] Ernst Bonek and Arpad Scholz. *Wellenausbreitung 2*. Institut für Nachrichtentechnik und Hochfrequenztechnik, Wien, 1993.

[4] Christopher J. Booth, editor. *The New IEEE Standard Dictionary of Electrical and Electronics Terms*. IEEE Press, Piscataway (New Jersey), fifth edition, 1995.

[5] D. C. Chang. Special issue. *IEEE Transactions on Antennas and Propagation*, 29, 1981.

[6] G.A. Dechamps. Microstrip microwave antennas. In *3rd USAF Symposium on Antennsas*, 1953.

[7] European Telecommunications Standards Institute (ETSI). *Radio Equipment and Systems; Wideband data transmission in the 2.4GHz ISM–band*, 1994.

[8] Josef Fuhl, Ernst Bonek, and Andreas F. Molisch. Smart antenna schemes for mobile radio applications: An overview. Technical report INTHF, Insitut für Nachrichtentechnik und Hochfrequenztechnik, Technical University Vienna, Gußhausstr. 25/389, A – 1040 Wien, Austria, January 1996.

[9] Kuldip C. Gupta and Abdelaziz Benella. *Microstrip Antenna Design*. Artech House, Inc., Dedham (Massachusetts), 1988.

[10] E. O. Hammerstad and O. Jensen. Accurate models for microstrip computer–aided design. *Digest IEEE MIT–S Internat. Microwave Symposium*, pages 407–409, 1980.

[11] R. F. Harrington. *Time–harmonic Electromagnetic Fields*. McGraw Hill, New York, 1961.

[12] Rosenberger Hochfrequenztechnik. *SMA Catalogue 9*. Tittmonig, Germany, 1990.

[13] Apisak Ittipiboon, Ron Oostlander, Yahia M. Antar, and Michel Cuhaci. A modal expansion method of analysis on aperture–coupled microstrip antenna. *IEEE Transactions on Antennas and Propagation*, AP–39(11):1567–1573, November 1991.

[14] Röhm Kunststoffe. *Rohacell Handbuch.* Röhm GmbH Chemische Fabrik, D – 64293 Darmstadt, Kirschenallee, Germany, 1995.

[15] Robert J. Mailloux. *Phased Array Antenna Handbook.* Artech House, Inc., Dedham (Massachusetts), 1993.

[16] C. Martín-Pascual. Hybrid technology for low cost active antenna. In *Workshop Proceedings: System Applications of Integrated Antennas*, pages 132–136, Bologna, Italy, September 1995. 25th European Microwave Conference.

[17] *Workshop Proceedings: System Applications of Integrated Antennas*, Bologna, Italy, September 1995. 25th European Microwave Conference.

[18] R. E. Munson. Conformed microstrip antennas–microstrip phased arrays. *IEEE Transactions on Antennas and Propagation*, 22:74–78, 1974.

[19] Allan Østergaard, Mikael Dich, and Ulrich Gothelf. A network model for the aperture coupled microstrip patch. *International Journal of Microwave and Millimeter–Wave Computer– Aided Engineering*, 3(4):326–339, 1993.

[20] David M. Pozar. Considerations for millimeter wave printed antennas. *IEEE Transactions on Antennas and Propagation*, 31(5):740–747, 1983.

[21] David M. Pozar. Microstrip antenna aperture–coupled to a microstrip–line. *Electronic Letters*, EL–21(2):49–50, January 1985.

[22] David M. Pozar. A reciprocity method of analysis for printed slot and slot–coupled microstrip antennas. *IEEE Transactions on Antennas and Propagation*, AP–34(12):1439–1446, December 1986.

[23] David M. Pozar and Daniel H. Schaubert. *Microstrip Antennas.* IEEE Press, Piscatayway (New Jersey), 1995.

[24] F. Rostan, E. Heidrich, and W. Wiesbeck. Design of aperture–coupled patch antenna arrays with multiple dielectric layers. In *Proceedings of 7th European Electromagnetic Structures Conference*, Torino/Italy, September 1993.

[25] F. Rostan, E. Heidrich, and W. Wiesbeck. High–performance C–band microstrip patch subarray with dual polarization capabilities. In *Proceedings of 7th European Electromagnetic Structures Conference*, Torino/Italy, September 1993.

[26] Georg Splitt. *Effiziente Rechenverfahren zur Analyse von komplexen Einzel– und Gruppenantennen in Streifenleitungstechnik.* PhD thesis, Deutsche Forschungsanstalt für Luft– und Raumfahrt, 1990.

[27] Georg Splitt. Guidelines for design of electromagnetically coupled microstrip patch antennas on two–layer substrates. *IEEE Transactions on Antennas and Propagation*, AP–38(7):1136–1140, July 1990.

[28] Georg Splitt. *MultiSTRIP v2.4 — User's Manual for the MultiSTRIP Program.* Fachhochschule Kiel, 1995.

[29] L. Warren Stutzman and Gary A. Thiele. *Antenna Theory and Design.* John Wiley & Sons, 1981.

[30] Peter L. Sullivan and Daniel H. Schaubert. Analysis of an aperture–coupled microstrip antenna. *IEEE Transactions on Antennas and Propagation*, AP–34(8):977–984, August 1986.

[31] Xian Hua Yang and Lotfollah Shafai. Characteristics of aperture coupled microstrip antennas with various radiating patches and coupling apertures. *IEEE Transactions on Antennas and Propagation*, AP–43(1):72–78, January 1995.

[32] Jean-François Zürcher. The SSFIP: A global concept for high–performance broadband planar antennas. *Electronic Letters*, EL–24(23):1433–1435, November 1988.

[33] Jean-François Zürcher and Fred E. Gardiol. *Broadband Patch Antennas.* Artech House, Inc., Norwood (Mass.), 1995.